HOKKAIDO UNIVERSITY

Title	Diffusion mechanism of water and ions in hardened cement pastes with different water to cement ratios
Author(s)	瀧谷, 啓晃
Degree Grantor	北海道大学
Degree Name	博士(工学)
Dissertation Number	甲第11885号
Issue Date	2015-03-25
DOI	https://doi.org/10.14943/doctoral.k11885
Doc URL	https://hdl.handle.net/2115/60948
Type	doctoral thesis
File Information	Hiroaki_Takiya.pdf

Hokkaido University Collection of Scholarly and Academic Papers : HUSCAP

Diffusion mechanism of water and ions in hardened cement pastes with different water to cement ratios

水セメント比の異なるセメント硬化体中の水およびイオンの拡散機構

Hiroaki TAKIYA

瀧谷　啓晃

Diffusion mechanism of water and ions in hardened cement pastes with different water to cement ratios

Hiroaki TAKIYA

Division of Energy and Environmental Systems, Graduate School of Engineering, Hokkaido University

2015

CONTENTS

Chapter 1
Introduction……..……..1
1.1 Nuclear energy and radioactive waste……1
1.2 Cement-based materials in radioactive waste disposal……6
1.2.1 Low-level radioactive waste (LLW)…...……6
1.2.2 High-level radioactive waste (HLW)……..8
1.3 Diffusion in cement-based materials……13
1.4 Objectives of the Thesis……21
1.5 Outline of the Thesis……..22
References……25

Chapter 2
Effect of a microstructure of hardened cement paste on diffusion behavior of water……30
2.1 Introduction……...30
2.2 Experimental methods……...……33
2.2.1 Preparation of HCP samples……33
2.2.2 Measurements of porosity and hydration degree……33
2.2.3 Non-steady diffusion method……...34
2.3 Results and discussion…..……39
2.3.1 Characteristics of HCP samples……39
2.3.2 Diffusion coefficients of HTO and $H_2{}^{18}O$……40
2.3.3 Temperature dependence of diffusion of HTO in HCP……42
2.3.4 Diffusion model of water in HCP……43
2.4 Conclusions……...63
References……65

Chapter 3
Water-to-cement ratio dependence of diffusion behavior of Na^+ and Cs^+ ions in hardened cement pastes…….……68
3.1 Introduction……..68
3.2 Experimental methods……...71
3.2.1 Preparation of HCP samples……71

3.2.2 Batch sorption……...71
3.2.3 Non-steady diffusion method……72
3.3 Results and discussion……...76
3.3.1 Sorption of Na^+ ion and Cs^+ ion on HCP……76
3.3.2 Diffusion coefficients of Na^+ ion and Cs^+ ion……...76
3.3.3 Activation energies for the diffusion of Na^+ ion and Cs^+ ion……77
3.3.4 Diffusion mechanism Na^+ ion and Cs^+ ion in HCP……..78
3.4 Conclusions……...…91
References……93

Chapter 4
Water-to-cement ratio dependence of diffusion behavior of Cl^- ion in hardened cement pastes……..95
4.1 Introduction……...95
4.2 Experimental methods……...97
4.2.1 Preparation of HCP samples……..…….97
4.2.2 Batch sorption……..97
4.2.3 Non-steady diffusion method…….97
4.3 Results and discussion……..……100
4.3.1 Sorption of Cl^- ion on HCP……100
4.3.2 Diffusion coefficients of Cl^- ion……..……101
4.3.3 Activation energy for the diffusion of Cl^- ion……102
4.3.4 Diffusion mechanism of Cl^- ion in HCP……102
4.4 Conclusions……..111
References……112

Chapter 5
Conclusions……114

Acknowldgements……118

Chapter 1
Introduction

1.1 Nuclear energy and radioactive waste

The prosperity of human society has been supported by mass consumption of energy. Coal had been used as a major energy source since the industrial revolution until giant oil fields were discovered in the Middle East in 1950's, resulting in the decline in oil price. Petroleum fuel displaced coal to become the major energy source, and the consumption of energy further increased. In 1970's, however, instability in the Middle East caused the energy crises, and significant petroleum shortage and elevated prices affected the economies of the major industrial countries. Vulnerabilities emerging from the uneven distribution of energy resources among countries were recognized, and the energy security, which is defined by International Energy Agency as "the uninterrupted availability of energy sources at an affordable price" [1], has become an issue of great importance. As the consumption of energy further increases, the world is now facing a thereat of the depletion of energy resources, which is expected to be more serious due to the economic growth of the developing countries and the increase in the global population. In addition, climate change, being caused by emissions of greenhouse gasses including carbon dioxide, has been added to a list of global energy issues. Thus, sustainability of future energy resources, on which economic growth and community prosperity depend, faces challenges including energy security, depletion of energy resources, and global warming.

Renewable energy and nuclear energy are alternatives to fossil fuels. Although

renewable energy can be semi-permanently used without emission of greenhouse gases, the initial cost or the generation cost is high. Wind and solar power generation is unstable due to their dependence on weather conditions. Building of hydraulic power plants has impacts on the natural environment. These disadvantages thwart the promotion of renewable energy. On the other hand, nuclear energy can provide energy at low cost without emission of greenhouse gases. In addition, uranium mines exist throughout the continents, including number of politically stable countries, which is favorable from an Energy Security perspective. For these reasons, Japanese energy policy recognizes nuclear power as an important base-load power source.

Although nuclear energy is an important alternative energy to fossil fuels, use of nuclear energy generates radioactive waste. In Japan, radioactive waste is classified broadly into low-level radioactive waste (LLW) and high-level radioactive waste (HLW), as shown in **Table 1-1**. LLW is further categorized into five types: very low-level radioactive waste, relatively lower activity waste, relatively higher activity waste, uranium waste, and transuranium (TRU) waste. The three types of LLW, very low-level, relatively lower, and relatively higher activity waste, are generated in association with the operation and decommissioning of nuclear power plants. The sum of their volume generated by 2009 was approximately 600,000 drums of 200 L [2]. The uranium waste is generated from uranium enrichment and uranium fuel fabrication facilities, and the volume generated by 2009 was approximately 104,000 drums of 200 L [2]. TRU waste is generated from nuclear fuel reprocessing facilities and mixed oxide (MOX) fuel fabrication facilities, and the volume generated by 2009 was approximately 145,000 drums of 200 L [2]. Another waste generated from nuclear fuel reprocessing

facilities is radioactive liquid waste, which is solidified in a glass matrix. In Japan, this is classified in HLW. By 2014, 2,167 containers of vitrified HLW have been processed [3], and they are stored in reprocessing facilities of Japan Nuclear Fuel Limited (JNFL) and Japan Atomic Energy Agency (JAEA). There are also spent fuels stored to be vitrified, which amount to be equivalent of approximately 22,600 canisters of vitrified HLW by 2014. It is necessary to safely treat and dispose of LLW and HLW in order to prevent radiation exposure. LLW and HLW are planned to be disposed of below the surface of the ground at varying depths depending on the radioactivity levels of the waste and the characteristics of radionuclides contained in the waste (e.g. half-life and type of radiation) in order to protect human health from the hazard posed by radioactive waste disposal, as shown in **Figure 1-1**.

Table 1-1 Generation, classification, and disposal method of radioactive waste.

			Examples	Origins of waste	Disposal methods
Low-level radioactive waste (LLW)	Waste from power reactors	Very low-level radioactive waste	• Concrete • Metals	Power Reactors	• Near-surface disposal (Trench Type)
		Relatively lower activity waste	• Liquid waste • Filters • Used equipment • Expendables		• Near-surface disposal (Concrete Pit Type)
		Relatively higher activity waste	• Control rods • Core internals		• Sub-surface disposal
	TRU waste		• Parts of fuel elements • Liquid waste • Filters	Reprocessing facilities MOX fuel manufacturing facilities	• Geological disposal • Sub-surface disposal • Near-surface disposal (Concrete Pit Type)
	Uranium waste		• Expendables • Sludge • Used equipment	Enrichment and fuel manufacturing facilities	• Sub-surface disposal • Near-surface disposal (Concrete Pit Type) (Trench Type) • Geological disposal
High-level radioactive waste (HLW)			• Vitrified waste	Reprocessing facilities	• Geological disposal

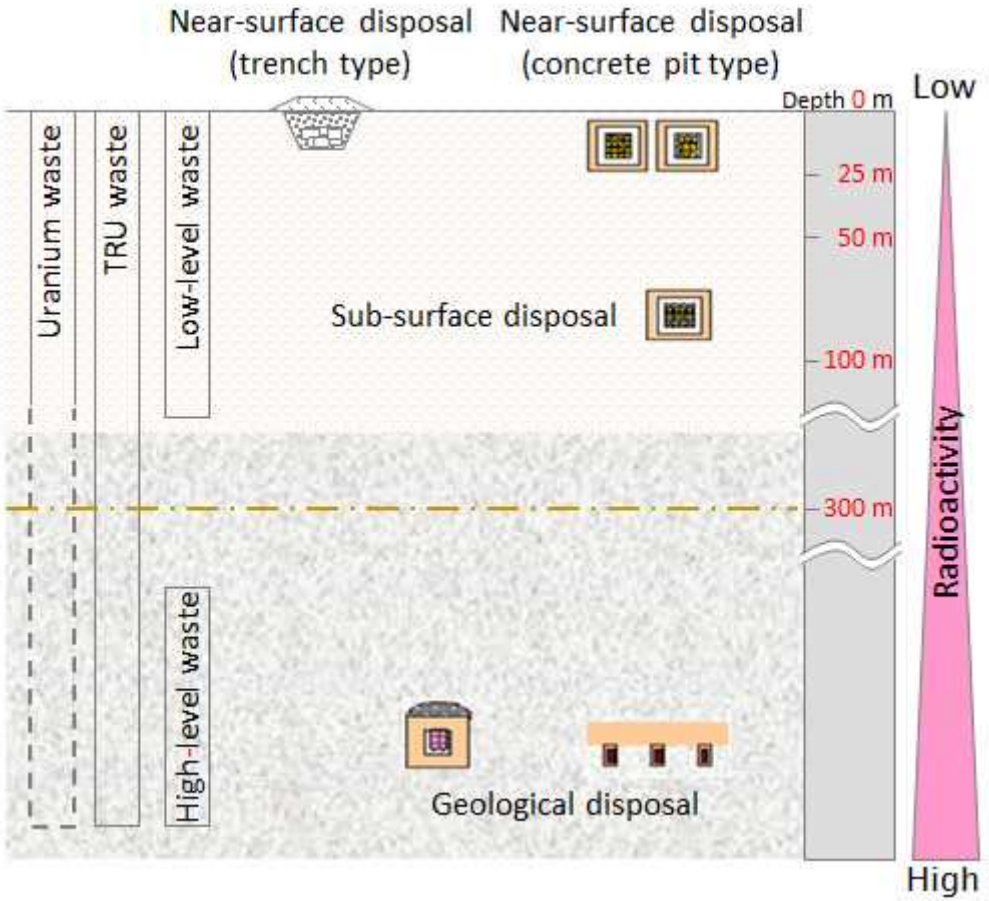

Figure 1-1 Disposal strategy for radioactive wastes in Japan [4].

1.2 Cement-based materials in radioactive waste disposal

1.2.1 Low-level radioactive waste (LLW)

The very low-activity waste of LLW is directly placed into trenches at shallow depth (near-surface disposal, trench type). The concept of the trench type disposal is shown in **Figure 1-2**. At trench type disposal facilities, rainfall will infiltrate through the soil cover and reach the waste. As a result, radionuclides may dissolve from the waste and migrate into the aquifer. The very low-activity waste includes a large quantity of concrete, which is a hardened mixture of cement and water with aggregates (e.g. sand and gravel), from, for example, decommissioning of the buildings and structures of nuclear power plants. Trench type disposal will be managed for about 50 years by monitoring the release of radioactive materials from the disposal facility and restricting the land use. After the management period, the land can be released to general use. A trench type disposal facility exists in a research facility of the Japan Atomic Energy Agency (JAEA).

The relatively lower-activity waste of LLW is solidified with cement in drums and is placed in concrete pit type disposal facilities at a shallow depth (near-surface disposal, concrete pit type). The concept of the concrete pit type disposal is shown in **Figure 1-3**. The concrete pit type disposal facilities are covered with bentonite in order to prevent water from penetrating. In addition, inner walls of the pits are made of porous concrete layer in order to drain water infiltrated from the outside. Bentonite and porous concrete have a function to prevent water from contacting with waste. When water reaches the waste and radionuclides in the waste are dissolved, cement-based materials (filler and pits) and bentonite are expected to retard the migration of radionuclides. The

concrete pit type disposal facility will be managed for 300-400 years by monitoring the release of radioactive materials and restricting the land use. After the management period, the land can be released to a general use. There is a concrete pit type disposal facility in Japan, which is managed by Japan Nuclear Fuel Limited (JNFL).

Relatively higher-activity waste of LLW is disposed of at a depth of 50-100 meters below the surface of the ground in order to maintain enough distance from general underground use (sub-surface disposal). The concept of the sub-surface disposal is shown in **Figure 1-4**. The cement-solidified radioactive waste in drums will be placed into concrete pits in disposal tunnels, and the space between the waste and the pit walls will be filled with cement-based materials. In addition, low diffusion layer (cement-based materials) and low permeable layer (bentonite) will be set up between disposal tunnels and concrete pits. The radionuclides may be released from the cement-solidified waste when groundwater infiltrates into the disposal facilities. Then, the cement-based materials (i.e. solidification, filler, and low diffusion layer) and bentonite are expected to play artificial barrier functions and exhibit low diffusivity and high sorptivity of radionuclides. Geological features are also expected to play a role of natural barrier with sorptivity. Leaching of alkaline components from cement-based materials including structural materials of tunnels and grout may deteriorate the barrier performance of cement-based materials, as well as the barrier performance of bentonite and geological features due to chemical alterations [5]. The sub-surface disposal facilities will be managed by monitoring the release of radioactive materials and restricting the land use. The management period is currently under consideration.

A part of TRU waste of LLW is disposed of in a deep geological formation at a

depth greater than 300 m in order to isolate the waste from the human environment for a long time (geological disposal), because of the relatively high radioactivity and the long half-lived radionuclides. The barrier system of geological disposal for TRU waste is basically similar to that of the sub-surface disposal, while no low diffusion layer may be set up. When groundwater infiltrates into disposal facilities and radionuclides may be released from the waste, the release of radionuclides into biosphere will be prevented by engineered (cement-based materials and bentonite) and natural (geological features) barriers. Similar to sub-surface disposal, leaching of alkaline components from cement-based materials including structural materials of tunnels and grout may cause the deterioration of the barrier performance of cement-based materials (filler and solidification), bentonite, and geological features [5].

A significant quantity of cement-based materials, as mentioned above, will be used in LLW disposal for purposes including solidifying agents, structures, and engineered barriers. Low diffusivity and high sorptivity of cement-based materials are expected to retard the migration of radionuclides. Leaching of alkaline components from cement-based materials, however, may be problematic in maintaining the barrier performance of cement-based materials, bentonite, and geological features. Therefore, it is very important to understand the migration mechanisms of radionuclides as well as alkaline component in cement-based materials for the safety assessment of disposal for LLW.

1.2.2 High-level radioactive waste (HLW)

The vitrified waste (HLW) will be disposed of in a deep geological formation

at a depth greater than 300 m in order to isolate the waste from the human environment for a long time (geological disposal), because of the high radioactivity and the long half-lived radionuclides. The concept of the geological disposal for HLW is shown in **Figure 1-5**. The release of radionuclides into biosphere is assumed to be caused by migrating through groundwater. The vitrified waste will be placed in carbon steel overpacks, and they will be surrounded by low permeable bentonite in order to prevent groundwater from contacting the waste for a certain period. When groundwater reaches the waste, the release of radionuclides from the vitrified waste is limited by the low dissolution rate of glass. When the dissolution takes place, bentonite and geological features are expected to retard the migration of radionuclides released from the vitrified waste by sorption and slow diffusion. In geological disposal of HLW, cement-based materials are also used in large quantities as structural materials of tunnels and grout. The leaching of alkaline components from the cement-based materials alkalizes groundwater around geological facilities. The high alkaline groundwater may deteriorate the barrier performance of bentonite and geological features [6]. Therefore, it is necessary to elucidate not only the performance of engineered and natural barriers but also the migration mechanisms of alkaline components in cement-based materials for the safety assessment of geological disposal for HLW.

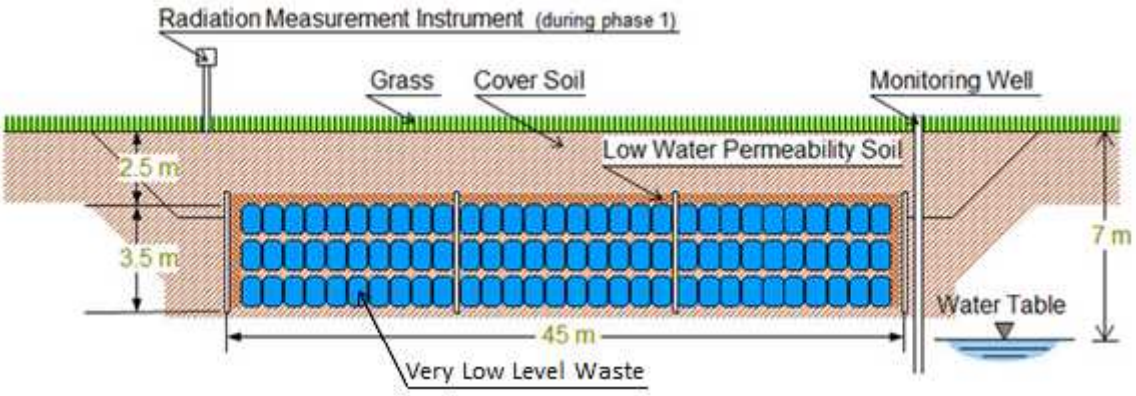

Figure 1-2 Concept of the trench type disposal system in Japan [4].

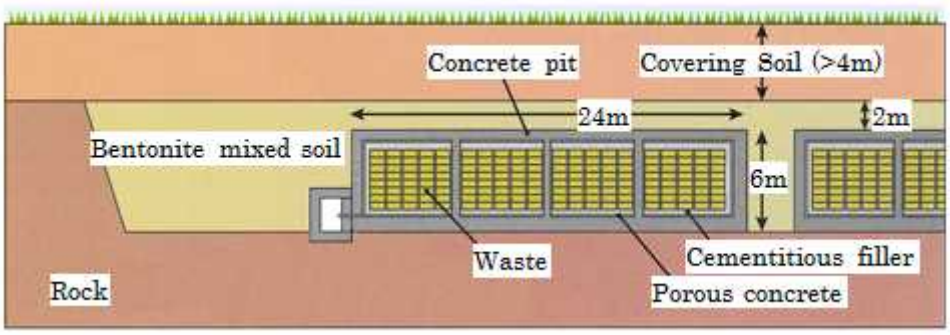

Figure 1-3 Concept of the concrete pit type disposal system in Japan [7].

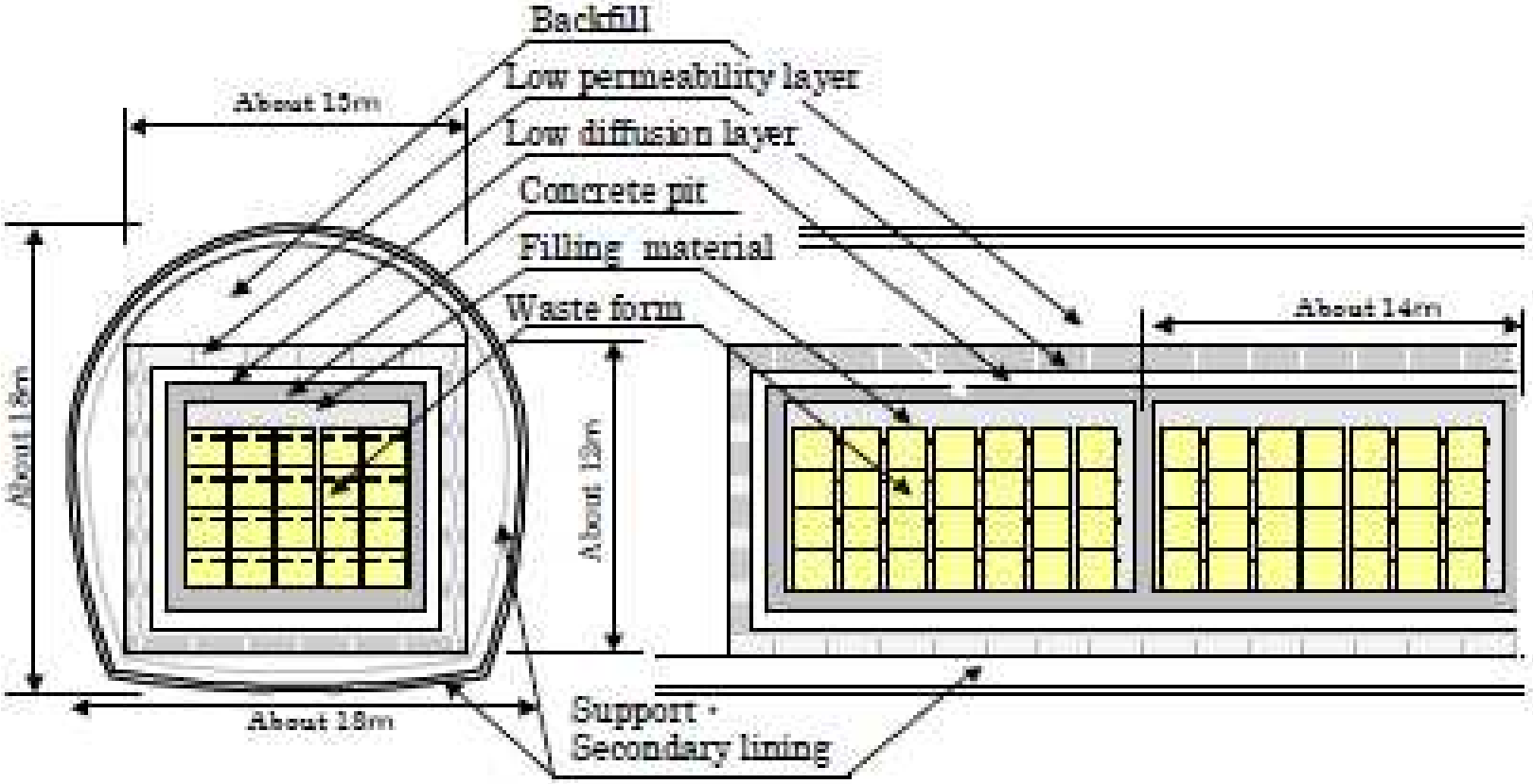

Figure 1-4 Concept of the sub-surface disposal system in Japan [8].

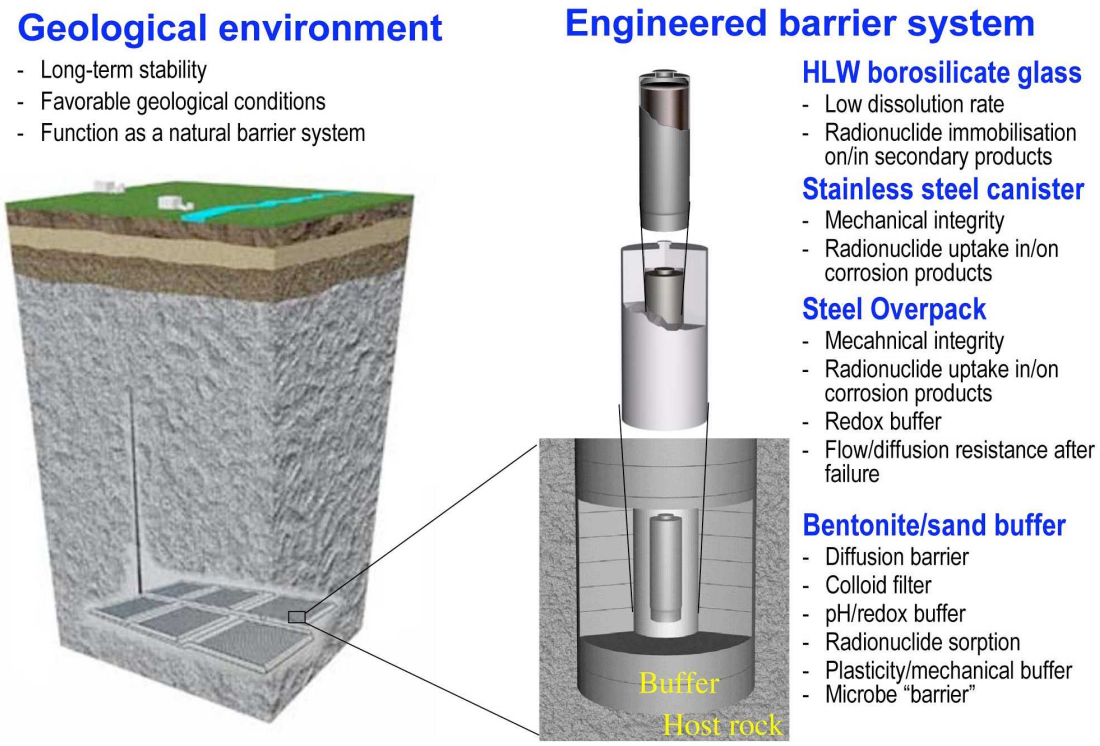

Figure 1-5 Concept of the geological disposal system in Japan with the components and the expected roles [9].

1.3 Diffusion in cement-based materials

Understanding the migration mechanisms of chemical species in cement-based materials is very important for reliable safety assessment for disposal of LLW and HLW, as mentioned in Section 1.2. Cement-based materials are hardened mixtures of cement and water with or without aggregates (e.g. sand and gravel) and other admixtures (e.g. fly ash and silica fume). Cement-based materials have a complex pore network consisting of pores in hardened cement paste (HCP), which is the hardened mixture of cement and water, and pores in interfacial transition zone (ITZ) between aggregates and cement paste. The ITZ is a more porous phase than the bulk HCP and usually has a width of 20-40 μm. Cement-based materials have low hydraulic conductivity, and chemical species diffuse in the complex pore network of cement-based materials. In order to elucidate diffusion mechanisms in cement-based materials, it is necessary to understand both the diffusion behavior in HCP and the influence of pores in ITZ.

The HCP has capillary pores with sizes in the range of a few nm to tens of μm, gel pores with diameters smaller than 10 nm, and cement particles of progressing degree of hydration [10]. Capillary pores are water-filled voids between cement particles, while gel pores are fine pores formed in hydrates. Initial volume of capillary pores can be estimated by a weight ratio of water to cement particles (i.e. water to cement (w/c) ratio). As the w/c ratio increases, pore size is enlarged in addition to the pore volume increase, as shown in **Figure 1-6** and **Figure 1-7**. As hydration proceeds, hydrates are formed in the voids between cement particles, and as the result, the volume and pore size of capillary pore contracts, as shown in **Figure 1-6** and **Figure 1-8**. The changes in w/c ratio and degree of hydration influence on the geometry (tortuosity and constrictivity) of

a complex network consisting of capillary and gel pores. However, it is difficult to directly measure and to numerically describe the pore geometry (tortuosity and constrictivity). From that reason, the diffusivity in HCP has been determined experimentally, and its relationship to the microstructure of HCP has been examined in two ways: i) experimental approach relating the diffusivity with macroscopic parameter (e.g. w/c ratio, porosity, etc.) and ii) analytical approach using a diffusion simulation in three-dimensional microstructure of HCP or using a mathematical diffusion model.

In experimental approach, diffusion experiments are performed using HCP with different w/c ratio (or different degree of hydration). The diffusivity in HCP (e.g. HTO [11-13], dissolved O_2 [14], Cs^+ ion [15, 16], Cl^- ion [14, 17, 18], I^- ion [15]) is positively correlated to w/c ratio. The positive correlation of diffusivity in HCP with w/c ratio has been related to changes in pore characteristics (pore geometry, pore size, and porosity). However, a relationship between diffusivity and pore geometry cannot be quantitatively discussed because of the difficulty in numerically determining pore geometry (tortuosity and constrictivity). The threshold pore width, which is the inflection point on the cumulative pore volume curve measured by mercury intrusion porosimetry (MIP), can be linearly related to diffusivity [19], but the detailed diffusion mechanism is unclear. In addition, the diffusivity in HCP can be also described as a (power) function of capillary porosity (or MIP porosity), which is a well-known empirical equation called "Archie's law". Numata et al. [11] reported that the effective diffusion coefficient (D_e) of HTO in HCP was related to the MIP porosity (ε_{MIP}) by the following equation:

$$D_e = 3.55\times10^{-11}\cdot\varepsilon_{MIP}^{0.947}. \quad (1\text{-}1)$$

Yamaguchi et al. [13] proposed the D_e value of HTO in HCP as a function of the volume fraction of capillary pores contributing on HTO transport (ε_{tra}):

$$D_e = 4.16\times10^{-10}\cdot\varepsilon_{tra}^{0.94\pm0.08}. \quad (1\text{-}2)$$

However, the percolation theory for capillary pores shows that the connectivity of capillary pores is lost in microstructure below approximately 18 % of capillary porosity (ε_{cap}) [20]. Based on the percolation theory, Garboczi and Bentz [21] quantitatively explained the relationship between the diffusivity of chloride ion in HCP and the microstructure by the following equation:

$$\frac{D_e}{D_v} = 0.001 + 0.07\varepsilon_{cap}^2 + H\left(\varepsilon_{cap}-0.18\right)\cdot 1.8\cdot\left(\varepsilon_{cap}-0.18\right)^2, \quad (1\text{-}3)$$

where H is the Heaviside's step function of $H(x)=0$ for $x\le 0$, and 1 for $x>0$. Although macroscopic approach using experimentally quantifiable data is useful and practical with a valid empirical equation (i.e. Archie's law), it does not elucidate the mechanisms of diffusion processes.

Analytical approach is based on numerical model studies relating microstructures to diffusion behaviors [12, 22]. Bejaoui and Bary [12] considered diffusion pathways consisting of a combination of capillary pores, low density calcium-silicate hydrate (C-S-H, which is a major component of OPC hydrates and includes gel pores), and high density C-S-H to fit to the diffusivity data obtained from experiment using HCP prepared at different w/c ratio. Kamali-Bernard et al. [22] modeled three-dimensional microstructure of HCP to simulate HTO diffusion and compared the results to experimental results. Both of the studies suggest the contribution of gel pores to diffusion of HTO in HCP, although the contribution of gel

pores to diffusion in HCP has not been yet experimentally demonstrated.

In addition to the above physical properties of HCP, the chemical properties of HCP can also influence the diffusion behavior of chemical species. Major hydrates in HCP are C-S-H, portlandite ($Ca(OH)_2$), ettringite (AFt phase) and monosulfate (AFm phase). C-S-H is an important solid phase which dominates over a half of the volume of completely hydrated cement, and has irregular layered structures consisting of C-S-H sheets. The surfaces of C-S-H have silanol groups ($\equiv Si-OH$), which is deprotonated to form negatively-charged silanol groups ($\equiv Si-O^-$) under high pH porewater caused by the dissolution of portlandite, NaOH, and KOH [23-25]. When Ca^{2+} ion concentration is high due to the dissolution of portlandite, the surface charge converts from negative to positive [24-26]. Ions of the opposite charge (counter-ions) of the surface charge can sorb on C-S-H, resulting in retardation of ionic diffusion. In fact, sorption of Na^+ [27], Cs^+ [28], and Cl^- ion [29] on C-S-H has been reported. The AFt phase and AFm phase, which make up 10-15 % of the volume of completely hydrated cement, can sorb anions (e.g. OH^-, Cl^-, I^-, IO_3^-, etc.) by exchanging with sulfate ions [10]. Thus, ionic diffusion can also be retarded by the interactions between ions and cement hydrates.

The influence of interactions between ions and cement hydrates on ionic diffusion has been examined experimentally. Page et al [17] suggested that the higher activation energy for effective diffusion of Cl^- ion in HCP than in bulk liquid water was caused by interactions between Cl^- ion and cement hydrates. Goto and Roy [30] suggested that, from the viewpoint of activation energy for effective diffusion, Na^+ and Cl^- ions interacted with surfaces of cement hydrates and the interaction of Na^+ ion with surfaces of cement hydrates was stronger than that of Cl^- ion. Ngala et al. [14] found

that the diffusivity of Cl^- ion in HCP differs from that of oxygen molecule, although oxygen molecule has the diffusivity similar to Cl^- ion in bulk liquid water and the size of oxygen molecule is similar to the diameter of Cl^- ion, suggesting that an interaction between Cl^- ions and charged pore walls or the electrical double layer on charged pore walls caused the difference in diffusivity. However, these studies did not discuss in detail types of interactions that occur between ions and cement hydrates, chemical properties of the hydrate surfaces where the interaction takes place, or effects of microstructures on the interactions, thus failed to elucidate the ionic diffusion mechanisms in HCP.

There is a need to investigate further on the relationship between diffusion behavior and the microstructure of HCP considering the more detailed pore geometry including gel pores, as well as the influence of interactions between ions and surfaces of cement hydrates on ionic diffusion. The nature of water confined in gel pores may be different from bulk water. For example, a quasi-elastic neutron scattering method [31, 32] detected the presence of water similar to supercooled bulk water in hydrated tricalcium silicate (C_3S), which is a major component of ordinary Portland cement (OPC). Similarly, a molecular dynamic simulation suggested that the structure of water on the surface of a C-S-H sheet was similar to that of supercooled bulk water [33]. The activation energy for water molecule diffusion in supercooled bulk water (44.4 kJ mol^{-1} [34]) is remarkably higher than in bulk liquid water (19.2 kJ mol^{-1} [35]). If the water similar to the supercooled bulk water is present in the gel pores, it may significantly affect diffusion behaviors and activation energy for diffusion of chemical species in HCP, which may allow us to clarify the contribution of gel pores to diffusion in HCP.

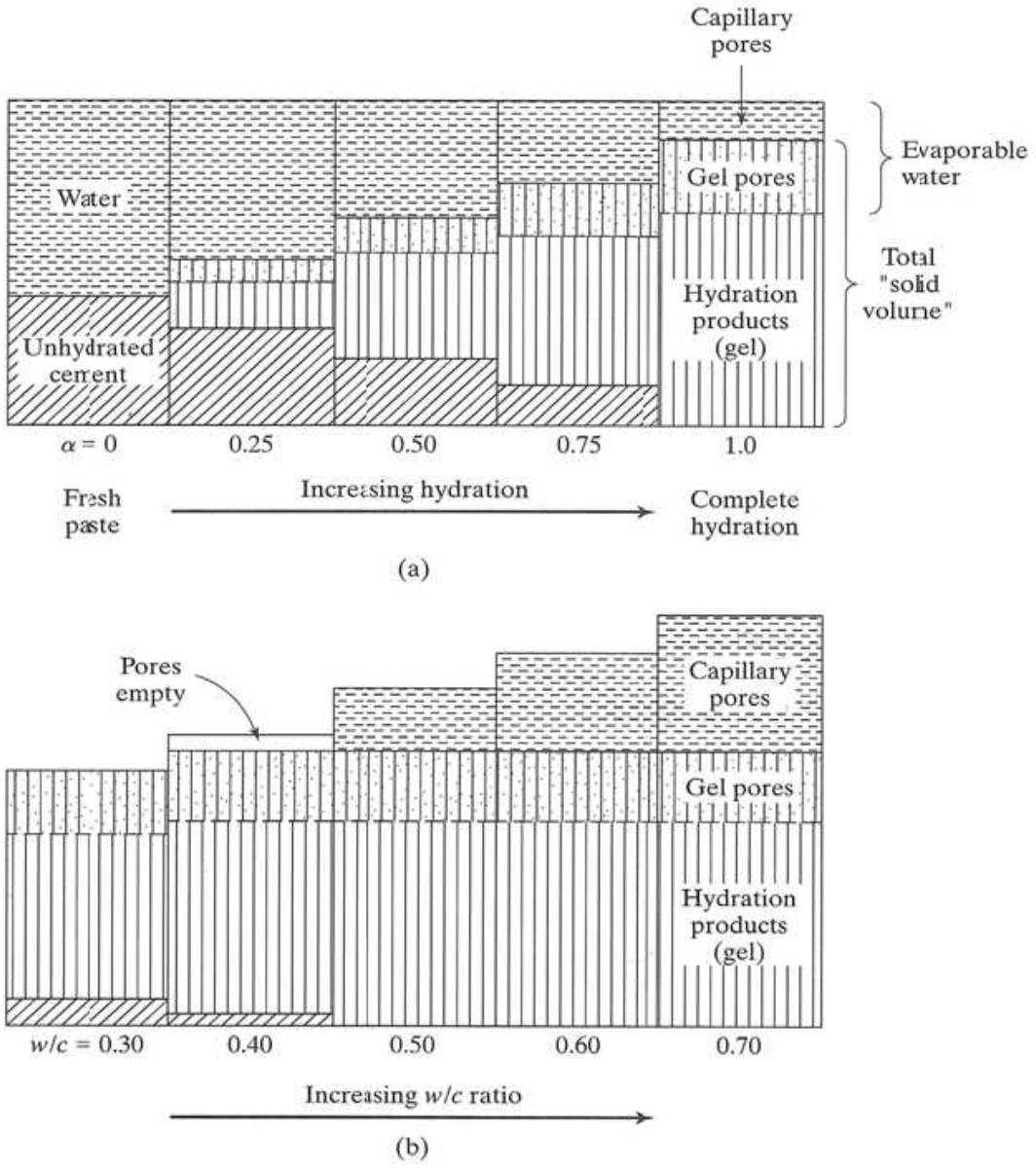

Figure 1-6 **Volume relationships among constituents of hydrated cement paste [10]: (a) changing degree of hydration (at w/c ratio of 0.50), (b) changing w/c ratio (under finishing hydration).**

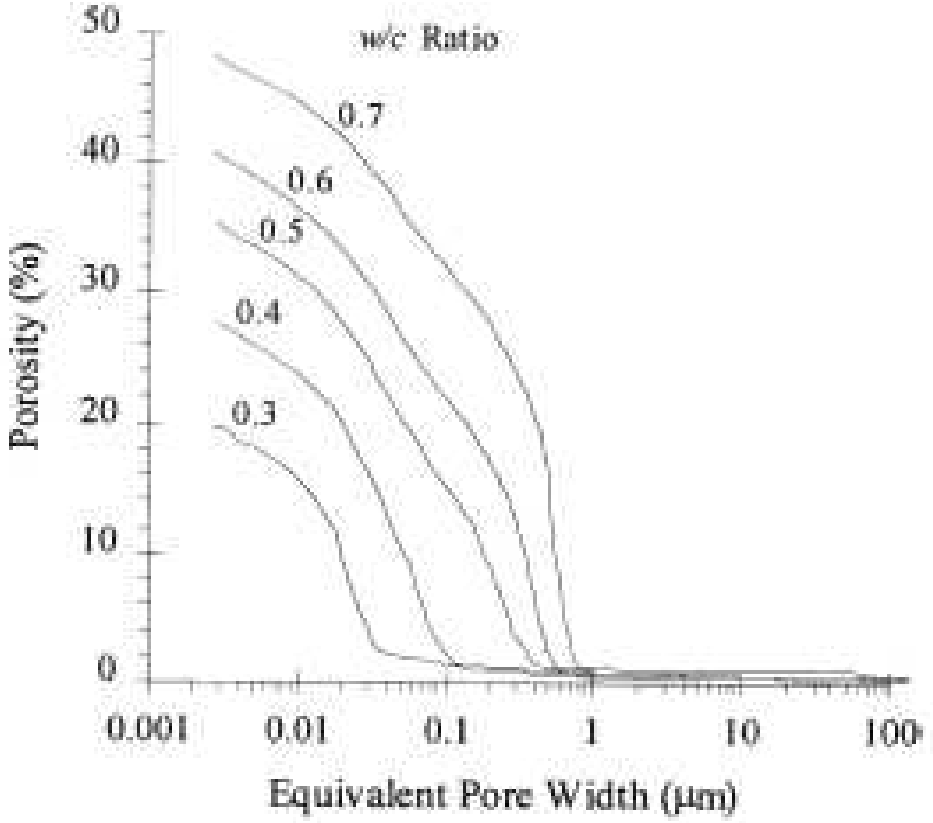

Figure 1-7 **The effect of w/c ratio on cumulative porosity by mercury intrusion porosimetry for paste cured for 7 days [36].**

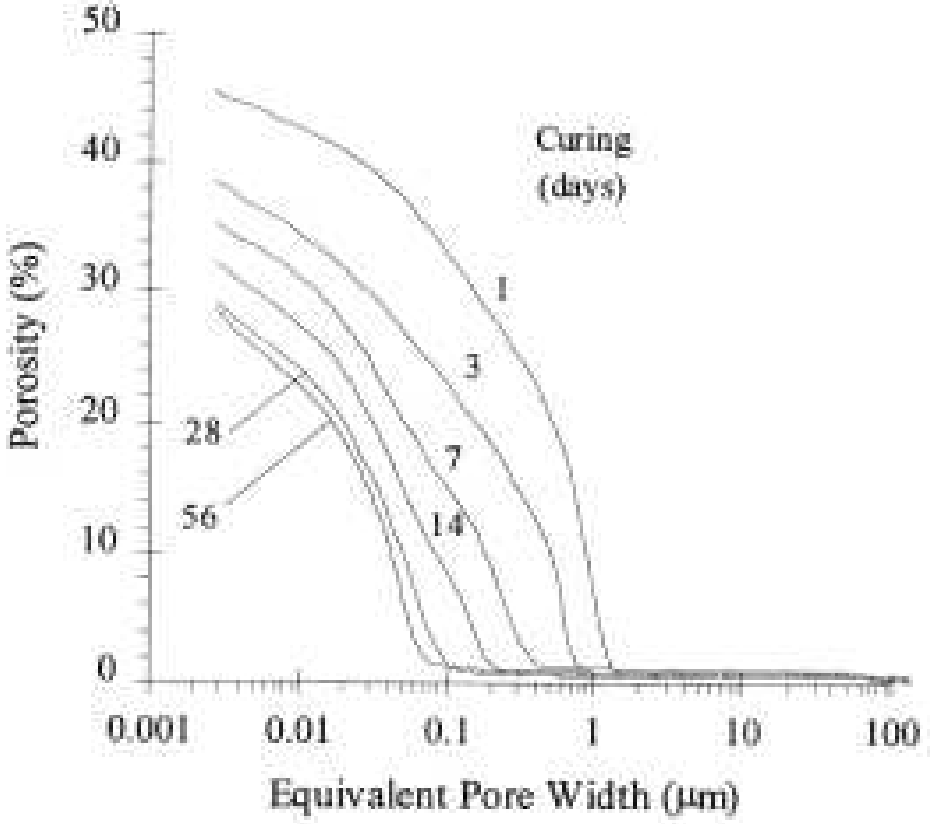

Figure 1-8 The effect of curing time on cumulative porosity by mercury intrusion porosimetry at w/c ratio of 0.50 [36].

1.4 Objectives of the Thesis

The barrier performance of cement-based materials is very important to prevent radionuclides release from waste into biosphere in the disposal for LLW. However, alkaline components leached from cement-based materials are possible to deteriorate the barrier performance of bentonite (a low permeable layer) and geological features due to dissolution and/or alteration of their constituent minerals, resulting in degradation of safety of the waste disposal systems. The geological disposal for HLW also has a similar risk of alkaline-caused deterioration of the barrier performance of bentonite and geological features because cement-based materials will be used in large quantities as structural materials of tunnels and grout. Therefore, it is necessary to elucidate diffusion mechanisms in cement-based materials, particularly in HCP, for reliable safety assessment of the disposal of both LLW and HLW.

Mass transport in HCP, as previously discussed, is controlled by a diffusion process because of the low hydraulic conductivity of HCP. The relationship between diffusivity of chemical species and pore structure of HCP has been examined by both experimental approach and analytical approach. In addition, the influence of electrochemical conditions of the surfaces of cement hydrates on ionic diffusion has been also studied experimentally. However, the detailed diffusion mechanisms in HCP have not been fully understood yet. In order to elucidate diffusion mechanisms in HCP, it is necessary to understand the contribution of gel pores and the influence of sorption behavior on diffusion.

In this study, firstly, a basic diffusion mechanism in HCP was discussed based on the pore geometry. By considering the nature of water confined in gel pores, the

contribution of gel pores to diffusion in HCP was examined by analyzing experimental results from the viewpoint of activation energy for diffusion. Two diffusion models were proposed based on the microstructure of HCP, and the degree of contribution of gel pores to diffusion was discussed by applying the model.

Next, ionic diffusion mechanisms in HCP were discussed for both cations and anions. Since ionic diffusion may be affected by electrochemical conditions of the surfaces of cement hydrates, interactions between ions and cement hydrates were considered based on sorption data and nature of hydrates. In addition, the influence of the interactions between ions and cement hydrates on ionic diffusion was discussed from diffusion and sorption data based on the detailed pore geometry including gel pores.

1.5 Outline of the Thesis

This thesis is intended to contribute in elucidating the diffusion mechanisms of water and ions in HCP, as a basic study for the assessment of the barrier performance of cement-based materials for LLW disposal and the influence of cement alkaline components on the barrier performance of bentonite and geological features. This thesis consists of five chapters.

In **Chapter 1**, background of this thesis and a concept of the radioactive waste disposal were introduced. Previous studies on the diffusion in HCP were reviewed, and the objectives of this thesis were explained.

In **Chapter 2**, diffusion behavior of water in HCP was examined by non-steady diffusion experiments. The apparent diffusion coefficients of water were obtained as

functions of w/c ratio using HTO and $H_2{}^{18}O$ as tracers. The dominant chemical species diffusing in HCP was confirmed to be H_2O molecule by comparing the apparent diffusion coefficients of HTO and $H_2{}^{18}O$. In addition, the activation energy for diffusion of HTO in HCP was determined from the temperature dependence of apparent diffusion coefficients. From the viewpoint of the w/c ratio dependence of the activation energy, two diffusion models consisting of capillary and gel pores were proposed based on the microstructure of HCP. The degree of a contribution of gel pores to diffusion was estimated by optimizing the model to fit with the experimental data for HTO. Finally, the influence of the changes in HTO diffusion pathways in complex pore network on diffusion behaviors was discussed.

In **Chapter 3**, diffusion behavior of Na^+ and Cs^+ ions in HCP was examined in the same way as HTO. The apparent diffusion coefficients of Na^+ and Cs^+ ions were obtained as functions of w/c ratio and temperature, and their activation energy for diffusion was determined from the temperature dependence of the apparent diffusion coefficients. In addition to diffusion experiments, the sorption of Na^+ and Cs^+ ions on HCP was studied by a batch sorption experiment. The diffusion behavior of Na^+ and Cs^+ ions in HCP was discussed based on the sorption and diffusion data, together using the model proposed in Chapter 2.

In **Chapter 4**, sorption and diffusion behavior of Cl^- ion in HCP was examined by a batch sorption experiment and a non-steady diffusion experiment. The distribution coefficients and apparent diffusion coefficients of Cl^- ion were obtained as functions of w/c ratio and temperature. The enthalpy for sorption and the activation energy for diffusion were determined from the temperature dependence of the distribution

coefficients and the apparent diffusion coefficients, respectively. The influence of sorption behavior on diffusion process and the diffusion behavior were discussed based on the sorption and diffusion data, together with findings obtained in Chapter 2.

In **Chapter 5**, main results of the thesis are summarized as conclusions.

References

[1] International Energy Agency HP
(http://www.iea.org/topics/energysecurity/subtopics/whatisenergysecurity/)

[2] Agency for Natural Resources and Energy HP
(http://www.enecho.meti.go.jp/category/electricity_and_gas/nuclear/rw/gaiyo/gaiyo01.html)

[3] Nuclear Waste Management Organization of Japan HP
(http://www.numo.or.jp/q_and_a/01/#qa04)

[4] Japan Atomic Energy Agency HP
(*http://www.jaea.go.jp/english/04/ntokai/backend/*)

[5] Japan Nuclear Cycle Development Institute and Federation of Electric Power Companies, JNC-TY1400 2005-001(1)/FEPC TRU-TR2-2005-03 in Japanese.

[6] Fujisaki K., Kubota S., Ueda H., Yamamoto T., Sugiyama D., Chida T., *Investigation of the methodology for selecting cementitious materials for the different components in the underground facility - Deriving component requirements and investigation of the weighting methodology*, Nuclear Waste Management Organization of Japan, NUMO-TR-13-07, 14-30 (2014).

[7] Japan Nuclear Fuel Limited HP
(*http://www.jnfl.co.jp/business-cycle/llw/structure.html*)

[8] JAEA, *Information Basis for Developing Comprehensive Waste Management System – US-Japan Joint Nuclear Energy Action Plan Waste Management Working Group Phase I Report – (Joint Research)*, Japan Atomic Energy Agency, JAEA-Research 2010-015 (2010).

[9] JNC, *H17: Development and management of the technical knowledge base for the geological disposal of HLW,* Japan Nuclear Cycle Development Institute, JNC TN1400 2005-022 (2005).

[10] Mindess S., Young J. F., Darwin D., *Concrete 2nd ed.*, Prentice Hall, Pearson Education Inc., Upper Saddle River, New Jersey, 57-91 (2003).

[11] Numata S., Amano H., Minami K., **"**Diffusion of tritiated water in cement materials," *J. Nucl. Mat.*, **171**, 373-380 (1990)

[12] Bejaoui S., Bary B., "Modeling of the link between microstructure and effective diffusivity of cement pastes using a simplified composite model," *Cem. Concr. Res.*, **37**, 469-480 (2007).

[13] Yamaguchi T., Negishi K., Hoshino S., Tanaka T., "Modeling of diffusive mass transport in micropores in cement based materials," *Cem. Concr. Res.*, **39**, 1149-1155 (2009).

[14] Ngala V. T., Page C. L., Parrott L. J., Yu S. W., "Diffusion in cementitious materials: II. Further investigation of chloride and oxygen diffusion in well-cured OPC and OPC/30% PFA pastes," *Cem. Concr. Res.*, **25**, 819-826 (1995).

[15] Atkinson A., Nickerson A. K., "The diffusion of ions through water-saturated cement," *J. Mat. Sci.*, **19**, 3068-3078 (1984).

[16] Nishi T., Kuriyama O., Matsuda M., Chino K., Kikuchi M., **"**Porosity and ion diffusivity of latex-modified cement," *Mat. Res. Soc.*, **176**, 109-114 (1990).

[17] Page C. L., Short N. R., Tarras A. E., "Diffusion of Chloride Ions in Hardened Cement Pastes," *Cem. Concr. Res.*, **11**, 395-406 (1981).

[18] Friedmann H., Amiri O., Aït-Mokhtar A., Dumarigue P., "A direct method for determining chloride diffusion coefficient by using migration test," *Cem. Concr. Res.*, **34**, 1967-1973 (2004).

[19] Halamickova P., Detwiler R. J., "Water permeability and chloride ion diffusion in Portland cement mortars: Relationship to sand content and critical pore diameter," *Cem. Concr. Res.*, **25**, 790-802 (1995).

[20] Bentz D. P., Garboczi E. J., "Percolation of phases in a three-dimensional cement paste microstructural model," *Cem. Concr. Res.*, **21**, 325-344 (1991).

[21] Garboczi E. J., Bentz D. P., "Computer simulation of the diffusivity of cement-based materials," *J. Mater. Sci.*, **27**, 2083-2092 (1992).

[22] Kamali-Bernard S., Bernard F., Prince W., "Computer modelling of tritiated water diffusion test for cement based materials," *Comp. Mat. Sci.*, **45**, 528-535 (2009).

[23] Chatterji S., Kawamura M., "Electrical double layer, ion transport and reactions in hardened cement paste," *Cem. Concr. Res.*, **22**, 774-782 (1992).

[24] Labbez C., Jönsson B., Pochard I., Nonat A., Cabane B., "Surface charge density and electrokinetic potential of highly charged minerals: Experiments and Monte Carlo simulation on calcium silicate hydrate," *J. Phys. Chem. B*, **110**, 9219-9230 (2006).

[25] Viallis-Terrisse H., Nonat A., Petit J.-C., "Zeta-potential study of calcium silicate hydrates interacting with alkaline cations," *J. Colloid Interface Sci.*, **244**, 58-65 (2001).

[26] Elakneswaran Y., Nawa T., Kurumisawa K., "Zeta potential study of paste blends with slag," *Cem. Concr. Res.*, **31**, 72-76 (2009).

[27] Hong S. –Y., Glasser F. P., “Alkali binding in cement pastes Part I. The C-S-H phase,” *Cem. Concr. Res.*, **29**, 1893-1903 (1999).

[28] Faucon P., Charpentier T., Henocq P., Petit J. C., Virlet J., Adenot F., “Interaction of alkalis (Cs^{+})with calcium silicates hydrates,” *Mat. Res. Soc. Symp. Proc.*, **506**, 551-559 (1998).

[29] Hirao H., Yamada K., Takahashi H., Zibara H., “Chloride binding od cement estimated by binding isotherms of hydrates,” *J. Adv. Concr. Technol.*, **3**, 77-84 (2005).

[30] Goto S., Roy D. M., “Diffusion of ions through hardened cement pastes,” *Cem. Concr. Res.*, **11**, 751-757 (1981).

[31] Fratini E., Faranoe A., Baglioni P., Bellissent-Funel M.-C., Chen S.-H., “Dynamic scaling of QENS spectra of glassy water in aging cement paste,” *Phys. A*, **304**, 1-10 (2002).

[32] Fratini E., Chen S.-H., Baglioni P., Bellissent-Funel M.-C., “Quasi-Elastic Neutron Scattering Study of Translational Dynamics of Hydration Water in Tricalcium Silicate,” *J. Phys. Chem. B*, **106,** 158-166 (2002).

[33] Youssef M., Pellenq R. J.-M., Yildiz B., “Glassy Nature of Water in an Ultraconfining Disordered Material: The Case of Calcium-Silicate-Hydrate,” *J. Am. Chem. Soc.*, **133**, 2499-2510 (2011).

[34] Price W. S., Hiroyuki I., Yoji A., “Self-Diffusion of Supercooled Water to 238 K Using PGSE NMR Diffusion Measurements,” *J. Phys. Chem. A*, **103**, 448-450 (1999).

[35] Wang J. H., Robinson C. V., Edelman I. S., "Self-diffusion and Structure of Liquid Water. III. Measurement of the Self-diffusion of Liquid Water with H^2, H^3 and O^{18} as Tracers," *J. Am. Chem. Soc.*, **75**, 466-470 (1953).

[36] Cook R. A., Hover K. C., "Mercury porosimetry of hardened cement pastes," *Cem. Concr. Res.*, **29**, 933-943 (1999).

Chapter 2
Effect of a microstructure of hardened cement paste on diffusion behavior of water

2.1 Introduction

Cement-based materials will be used as an engineered barrier to retard the migration of radionuclides in the disposal facilities of low-level radioactive waste (LLW). The barrier performance of cement-based materials may be degraded by leaching of cement alkaline components (NaOH, KOH, and $Ca(OH)_2$). In addition, alkaline solution leached from cement-based materials may deteriorate the performance of other barrier materials including bentonite and geological features [1]. The influence by alkaline solution on bentonite and geological features is also an important issue for geological disposal of high-level radioactive waste (HLW) [2], because cement-based materials will be used in large quantities as structural materials of tunnels and grout in the HLW disposal systems. Therefore, it is very important to elucidate migration mechanisms of chemical species in cement-based materials for reliable safety assessment of disposal for LLW and HLW.

The migration in hardened cement paste (HCP) is controlled by diffusion because of the low hydraulic conductivity of HCP. The diffusion mechanisms in HCP are still ambiguous due to the complexity of the pore network in HCP where diffusion takes place and the interactions between ions and cement hydrates (e.g. sorption and electrostatistical interaction). Using tritiated water (HTO) as a tracer has an advantage of being electrically neutral (non-charged), making it inert to cement hydrates [3, 4],

and as the result, diffusion behavior of HTO only reflects the complexity of pore geometry of HCP. The relationship between the diffusivity and porosity, which is well-known as an empirical equation called “Archie’s law”, is often used [5, 6], but , it does not provide the mechanistic information on the diffusion in HCP. Numerical model studies relating diffusion behaviors to microstructures [7, 8] suggested the contribution of gel pores to diffusion of HTO in HCP, but the contribution of gel pore has not been demonstrated experimentally yet. In order to understand diffusion mechanisms of HTO in HCP, the contribution of gel pores to diffusion in HCP needs to be examined and more detailed pore geometry including gel pores may need to be considered.

In this Chapter, a relationship between diffusion behaviors of HTO and the microstructure of HCP was discussed from the apparent diffusion coefficients of HTO obtained from diffusion experiment using HCP samples prepared with different w/c ratios. A tracer of $H_2{}^{18}O$ was also used in the diffusion experiments in order to confirm that diffusion of dissociation products of HTO was negligibly small and HTO was the dominant chemical species diffusing in HCP. The activation energy for HTO diffusion was determined at each w/c ratio. Diffusion pathways were considered with two kinds of simple models consisting of capillary and gel pores, one model with capillary and gel pores connected in series in the direction of diffusion, and the other model with capillary and gel pores constituting independent diffusion pathways without being connected. The estimate of the volume ratio of gel pores to total pores was obtained for both of the models by optimizing the model to fit with all of the experimental data with the purpose of gaining insight into diffusion pathways and the pore geometry in HCP, especially on the significance of the contribution of gel pores. Based on the new

approach of determining the diffusion coefficients as a function of both w/c ratio and temperature, the influence of the changes in HTO diffusion pathways in complex pore network on diffusion behavior was discussed.

2.2 Experimental methods

2.2.1 Preparation of HCP samples

Ordinary Portland cement (OPC) powder (Japan Cement Association) was used to prepare HCP samples. The composition of OPC powder used is shown in **Table 2-1**. The OPC powder was mixed with deionized water at w/c ratio of 0.36, 0.40, 0.45, 0.50, and 0.60 (in weight). The mixtures were settled for 30 minutes at 303 K before they were remixed. This procedure was repeated until no water seeped to the surface of the cement paste due to settling. The mixtures were then poured into cylindrical polyethylene molds of 24.5 mm in inner diameter and 60 mm in height. They were covered with a sheet of polyethylene to prevent moisture loss and were settled for approximately 1 day at room temperature. After removing the molds, HCP rods were cured for 90 days at 323 K in the cement-equilibrated water, which was prepared by mixing 2 dm^3 of deionized water with 0.2 kg of OPC powder and settling for more than 2 days.

2.2.2 Measurements of porosity and hydration degree

Total porosity and degree of hydration of HCP samples were determined from the weight loss by drying a water-saturated sample and igniting after drying. Disk-type specimens of 24.5 mm in diameter and 5.0 mm in thickness were cut from the center of HCP rods with a water-cooled diamond blade. Specimens were saturated by submerging in the cement-equilibrated water in a vacuum desiccator to determine the water-saturated weight (m_1). Specimens were dried in an oven for more than 1 week at 333 K [9] to determine the dried weight (m_2). After drying in the oven, they were

pulverized to less than 75 μm in particle size, and 3.0 g of the pulverized specimens were heated in an electric furnace for more than 1 hour at 1273 K [10] to determine the weight of the ignition residue (m_3).

Total porosity (ε_{tot}) and degree of hydration (α) [11] were calculated by the following equations;

$$\varepsilon_{tot} = \frac{m_p}{\rho_w V}, \tag{2-1}$$

and

$$\alpha = \left(\frac{m_c / m_s - L_C}{1 - L_C} \right) \Big/ \gamma, \tag{2-2}$$

where m_p is the amount of porewater ($m_1 - m_2$), m_s is the weight of pulverized HCP sample ignited in an electric furnace (3.0 g), m_c is the amount of water chemically bound in hydrates ($m_s - m_3$), V is the volume of a disk-type specimen (2.36 cm^3), ρ_w is the water density at 293 K (0.998 g cm^{-3}), L_C is the rate of mass loss including decarboxylation by ignition of cement powder in an electric furnace (6.2×10^{-3} for OPC used in this study), and γ is the ratio of water consumed for complete hydration to 1 g of anhydrous cement (0.23). Capillary porosity (ε_{cap}) was calculated by the following equation [12], and gel porosity (ε_{gel}) was calculated by subtracting ε_{cap} from ε_{tot}:

$$\varepsilon_{cap} = \frac{w/c - 0.36\alpha}{w/c + 0.32}. \tag{2-3}$$

2.2.3 Non-steady diffusion method

The dependence of the apparent diffusion coefficient of HTO on w/c ratio and

temperature was studied by a non-steady diffusion experiment with an instantaneous source. A specimen of 40 mm in height and 24.5 mm in diameter was cut out from the center of a HCP rod with a water-cooled diamond blade. After they were saturated with the cement-equilibrated water in a vacuum desiccator, a slight amount of HTO tracer (PerkinElmer Life & Analytical Sciences) solution was applied to the flat surface of a HCP specimen. Two HCP specimens were placed together in contact, and were covered with rubber and plastic paraffin films to prevent drying (**Figure 2-1 (a)**). They were kept at temperature of 293 K, 303 K, 313 K, and 323 K for the duration of experiment.

A non-steady diffusion experiment with a constant source was conducted in order to compare the apparent diffusion coefficients of HTO and $H_2{}^{18}O$ and to estimate the volume of pores accessible for HTO and $H_2{}^{18}O$. The specimen was cut out similarly from the center of a HCP rod, and all of the surfaces except for the top were sealed by resin. After being saturated with cement-equilibrated water, it was immersed in the source solution for the duration of the diffusion experiment for 5days at 303 K (**Figure 2-1(b)**). During diffusion period, the changes in the tracer concentration in the source solution were confirmed to be less than 1 %. The source solution was prepared by adding a slight amount of HTO or $H_2{}^{18}O$ (Cambridge Isotope Laboratories, Inc.) in cement-equilibrated water.

After the diffusion period, the specimen was sliced into 1.0 mm thick sections from the contacting surface with a water-cooled diamond blade. The wafers were pulverized and immersed in 1.5-2.5 ml of cement-equilibrated water at room temperature for more than 1 week until HTO or $H_2{}^{18}O$ in the wafer was released into cement-equilibrated water. The amount of the tracer applied in the instantaneous-source

diffusion experiment was confirmed to be extracted in this procedure to satisfy the material balance of HTO. After filtration through a hydrophilic polytetrafluoroethylene (PTFE) type membrane filter with 0.45 μm pore size (25HP045AN, ADVANTEC), the concentration of HTO or $H_2{}^{18}O$ in the supernatant was determined as a function of distance from the plane where HTO was applied or the source solution of HTO and $H_2{}^{18}O$ contacted with the specimen. The radioactivity of HTO in the supernatant was measured using a liquid scintillation counter (LSC-5100, Aloka, Ltd.). For the analysis of $H_2{}^{18}O$, the mole fraction of O-18 in the supernatant was calculated from the oxygen isotopic ratio ($\delta^{18}O$) which was measured by a mass spectrometer using the exchange of O-18 between H_2O and CO [13].

Table 2-1 Chemical compositions of OPC used in experiments (Japan Cement Association).

Chemical Analysis	(%)
Calcium oxide (CaO)	65.02
Silicon dioxide (SiO_2)	21.36
Aluminum trioxide (Al_2O_3)	5.28
Ferric trioxide (Fe_2O_3)	2.66
Sulfur trioxide (SO_3)	2.08
Sodium oxide (Na_2O)	0.29
Potassium oxide (K_2O)	0.48
Magnesium oxide (MgO)	1.46

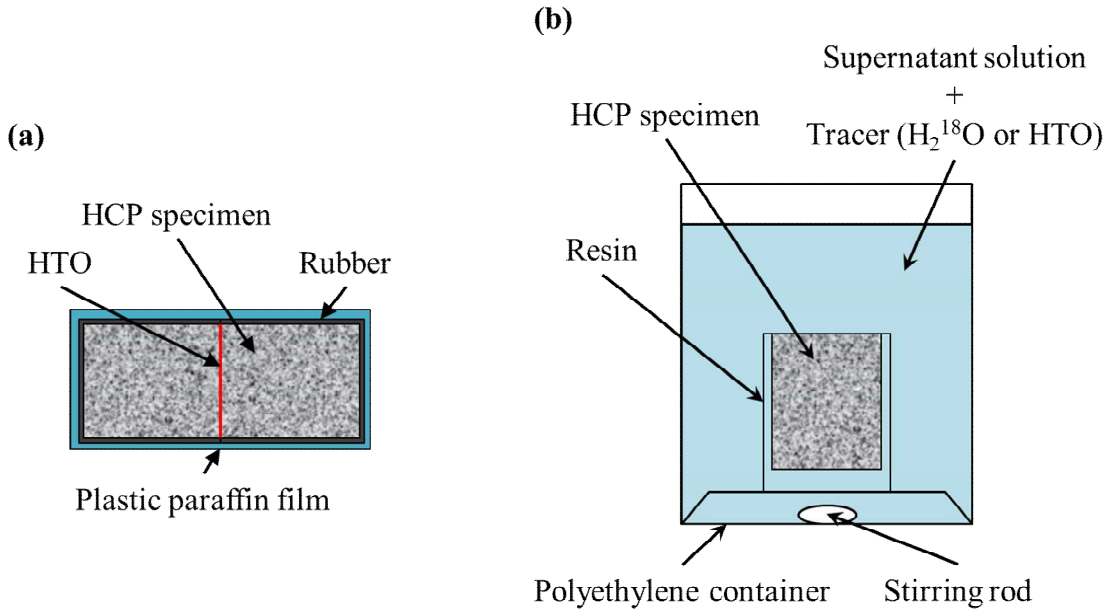

Figure 2-1 **Schematic diagrams of non-steady diffusion experimental system (Left: HTO instantaneous source, Right: $H_2{}^{18}O$ or HTO constant source).**

2.3. Results and discussion

2.3.1. Characteristics of HCP samples

The porosity (ε_{tot}, ε_{cap}, and ε_{gel}) and degree of hydration (α) are shown in **Table 2-2**, together with water contents in HCP specimens (m_p and m_c) determined from weight loss after drying and igniting. The value of α increased with an increase in w/c ratio, as previously reported [10, 14, 15]. The values of ε_{tot} and ε_{cap} increased with an increase in w/c ratio, while the value of ε_{gel} decreased because of the reduction of the volume of cement paste per unit volume. These changes indicated that the volume of larger pores increased as w/c ratio increased.

Pores in HCP can be divided into two zones; pores that are accessible for migration and pores that are not. The porosity of the accessible pores is defined as effective porosity (ε_{eff}), and is generally estimated from the total amount of a tracer that penetrates into a water-saturated porous media by diffusion. In this study, the tracer concentration ($C(\Delta x,t)$) in the porewater in the thin HCP slice closest to the source solution was assumed to be equal to the tracer concentration (C_0) in the source solution ($C_0 = C(\Delta x,t)$). The concentration of the tracer per unit volume of the HCP slice ($C_s(\Delta x,t)$) was obtained from the concentration profile acquired in the constant-source diffusion experiment. Using the volume of the HCP slice (ΔV), the amount of the tracer (A) in the HCP slice is represented as:

$$A = C(\Delta x,t)\cdot \Delta V \cdot \varepsilon_{eff} \tag{2-4}$$

or

$$A = C_s(\Delta x,t)\cdot \Delta V\,. \tag{2-5}$$

From the above assumption ($C_0 = C(\Delta x, t)$), Equations (2-4), and (2-5), the ε_{eff} value is calculated by the following equation:

$$\varepsilon_{eff} = \frac{C_s(\Delta x, t)}{C_0}. \tag{2-6}$$

The values of ε_{eff} are shown in **Table 2-2**. The values of ε_{eff} were larger than ε_{cap} and were close to ε_{tot}, suggesting that HTO and $H_2{}^{18}O$ can enter into gel pores during diffusion.

2.3.2 Diffusion coefficients of HTO and $H_2{}^{18}O$

Figure 2-2 shows a typical concentration profile of HTO in HCP obtained from the instantaneous-source diffusion experiment. The apparent diffusion coefficient (D_a) was determined by fitting the following analytical equation to the concentration profile [16]:

$$C(x,t) = \frac{M}{2\sqrt{\pi D_a t}} \exp\left(-\frac{x^2}{4D_a t}\right), \tag{2-7}$$

where M is the amount of HTO tracer initially applied (cpm), t is diffusion time (s), and x is penetration depth (m). The concentration profiles in all cases of w/c ratio and temperature were well reproduced by Equation (2-7). The values of D_a obtained are shown in **Table 2-3**. The D_a values ranged from 1.1×10^{-11} m^2 s^{-1} to 1.7×10^{-10} m^2 s^{-1} at w/c ratio from 0.36 to 0.60 and at diffusion temperature from 293 to 323 K.

Figure 2-3 shows typical concentration profiles of HTO and $H_2{}^{18}O$ in HCP obtained from the constant-source diffusion experiment. The apparent diffusion coefficient was determined by fitting the following analytical equation to the

concentration profile [16]:

$$C(x,t) = C_0 erfc\left(\frac{x}{\sqrt{4D_a t}}\right), \quad (2\text{-}8)$$

where C_0 is the initial concentration of HTO (cpm m^{-3}) or $H_2{}^{18}O$ (mole fraction unitless) in the source solution. Similar to the results from instantaneous-source diffusion experiments, the concentration profiles for HTO and $H_2{}^{18}O$ at all w/c ratios were well reproduced by Equation (2-8). The values of D_a obtained are shown in **Table 2-3**. The D_a values for HTO and $H_2{}^{18}O$ ranged from 2.6×10^{-11} m^2 s^{-1} to 9.2×10^{-11} m^2 s^{-1} at w/c ratio from 0.36 to 0.60 at 303 K.

Figure 2-4 shows the dependence of the apparent diffusion coefficient on w/c ratio at 303 K. No significant difference was observed between the D_a values of HTO and $H_2{}^{18}O$, suggesting that the influence of dissociation of HTO and $H_2{}^{18}O$ on the diffusion is negligible: HTO and $H_2{}^{18}O$ diffuse as water molecules even in alkaline porewater in HCP.

The diffusivity in porous media is related to the porosity (ε) by an empirical equation (i.e. Archie's law):

$$D_e / D_v = \varepsilon^m, \quad (2\text{-}9)$$

where D_e is the effective diffusion coefficient in porous media, D_v is the self-diffusion coefficient in bulk liquid water (2.7×10^{-9} m^2 s^{-1} for HTO and 3.1×10^{-9} m^2 s^{-1} for $H_2{}^{18}O$ at 303 K, which were calculated from self-diffusion coefficients at 298 K and activation energies [17]) and m is the cementation factor, which is a fitting parameter. Since the sorption of water on cement hydrates is negligible [3, 4], the apparent diffusion coefficient is equal to the effective diffusion coefficient divided by

ε_{tot} or ε_{cap}. The D_a/D_v value plotted against ε_{tot} and ε_{cap} is shown in **Figure 2-5 (a) and (b)**, respectively. The ε_{tot} value can reproduce the D_a/D_v value by the power function (**Figure 2-5 (a)**) and the exponent was approximately 4.2. Similarly, the D_a/D_v values fitted with the power function of the ε_{cap} (**Figure 2-5 (b)**). The values of D_a/D_v deviated from the power function at lower ε_{cap} values.

2.3.3. Temperature dependence of diffusion of HTO in HCP

Figure 2-6 shows the apparent diffusion coefficient of HTO as a function of temperature. The plots were well reproduced at all w/c ratios by the Arrhenius equation:

$$D_a = B\exp\left(-\frac{E_a}{RT}\right), \tag{2-10}$$

where E_a is the activation energy for diffusion (kJ mol^{-1}), B is an arbitrary constant, R is the gas constant (8.31 J mol^{-1} K^{-1}), and T is absolute temperature (K). The values of E_a obtained at w/c ratio of 0.36, 0.45, and 0.60 were 31.3±2.7 kJ mol^{-1}, 22.9±1.3 kJ mol^{-1}, and 21.5±3.1 kJ mol^{-1}, respectively, as shown in **Table 2-3**. **Figure 2-7** shows the activation energy as a function of w/c ratio. The E_a value of 21.5 kJ mol^{-1} obtained at w/c ratio of 0.60 was close to that in bulk liquid water (19.2 kJ mol^{-1} [17]). The activation energy increased as w/c ratio decreased. The E_a value of 31.3 kJ mol^{-1} at w/c ratio of 0.36 was significantly higher than 19.2 kJ mol^{-1}. This finding indicates that the dominant diffusion process at lower w/c ratio is different from diffusion in bulk liquid water.

Higher activation energy of 44.4 kJ mol^{-1} has been reported for the diffusion of water molecules in supercooled bulk water [18]. Water similar to supercooled bulk

water (hereafter “confined water”) has been identified in hydrated tricalcium silicate (C_3S, which is a major component of OPC) by a quasi-elastic neutron scattering method [19, 20] and on the surface of a calcium-silicate-hydrate sheet (C-S-H, which is a major component of OPC hydrates with the similar layer structure to tobermorite or jennite) by molecular dynamics simulation [21]. If the higher activation energy can be attributed to the confined water, HTO may diffuse in at least two different types of water in HCP, i.e. the confined water (region 1) and the bulk liquid water (region 2). Changes in the apparent diffusion coefficients and the activation energy as a function of the w/c ratio may be explained by the volume ratio of the region 1 and the region 2, and microstructure of the two regions where HTO diffuses.

2.3.4. Diffusion model of water in HCP

Simple models for the diffusion pathways of HTO in HCP are considered in order to explain the changes in apparent diffusion coefficients and activation energies with an increase in w/c ratio, i.e. an increase in w/c ratio from 0.36 to 0.60 resulted in an increase of apparent diffusion coefficients from 2.0×10^{-11} m^2 s^{-1} to 9.9×10^{-11} m^2 s^{-1} at 303 K and a decrease in activation energies from 31.3 kJ mol^{-1} to 21.5 kJ mol^{-1}. These changes may be attributed to differences in pore structures caused by an increase in w/c ratio. As described in section 2.3.3, if confined water causes higher activation energy of 31.3 kJ mol^{-1}, pores in HCP can be divided into regions filled with confined water (region 1) and bulk liquid water (region 2). A molecular dynamics simulation by Youssef et al. indicates the formation of water similar to supercooled bulk water up to 0.42 nm in thickness and the confinement of water molecules persisting up to 1.0 nm

from the surface of a C-S-H sheet [21]. According to this simulation, the confined water (i.e. region 1) occupies up to at least 0.42 nm in thickness from the surface of a C-S-H sheet, and may extend up to around 1.0 nm: pore water existing further away from C-S-H sheets is bulk liquid water (region 2). Gel pores are formed in hydrates, whose major constituent is C-S-H, and have radius smaller than 5 nm [12]. When the radius of a gel pore is similar to the thickness of confined water on the surface of hydrate sheets, most of gel pores may be considered as region 1. On the other hand, capillary pores have significantly greater radius between hydrated cement particles than gel pores. For example, the distribution of capillary pore radius determined by an MIP measurement is dominated by radius between 10 nm and 30 nm at w/c ratio between 0.30 and 0.70 [10]. Although region 1 may exist as a thin layer on the inner-surfaces of capillary pores, capillary pores may be assumed to be filled only with bulk liquid water (region 2) since the volume of region 1 is negligible compared to region 2.

Diffusion of HTO is considered to occur through only capillary pores [6] or through both capillary pores and gel pores [7, 8, 22]. However, if HTO diffuses only in capillary pores filled with bulk liquid water (region 2), the activation energy should remain constant. The activation energies determined in this study were not constant, suggesting that the contribution of a diffusion process that has higher activation energy, such as that in confined water (region 1), is substantial enough compared to the diffusion in bulk liquid water (region 2). In order for the diffusion in region 1, which has the diffusivity (e.g. 1.6×10^{-10} m^2/s in supercooled bulk water at 238 K [18]) approximately one order of magnitude smaller than the diffusivity in bulk liquid water (2.4×10^{-10} m^2/s [17]), to raise the activation energy for the entire HCP system, HTO

has to pass through region 1 in the case when the diffusion pathway consisting of region 1 and region 2 connected in series in the direction of diffusion (case 1, the serial model), or region 1 needs to have significant enough volume in the case when the pore network comprises region 1 and region 2 as independent diffusion pathways (case 2, the parallel model). Basic module of the microstructure for the serial model (case 1) is shown in **Figure 2-8 (a)**, and the parallel model (case 2) is shown in **Figure 2-8 (b)**. For simplification, the sum of the areas of capillary pores and that of gel pores were assumed to be constant at any cross sections perpendicular to the direction of diffusion.

In the serial model (**Figure 2-8 (a)**), region 1 and region 2 are arranged up in series in a pathway in the direction of diffusion: HTO diffuses through region 1 and region 2 in series. The longer the diffusion path of region 1, the more significant the influence of region 1 on apparent diffusion coefficients and activation energies becomes. In the serial model, the ratio of the length of the path of region 1 to the total length of the diffusion pathway is equal to the ratio of gel porosity to total porosity. In the parallel model (**Figure 2-8 (b)**), region 1 and region 2 constitute independent diffusion pathways: HTO diffuses only through region 1 if HTO enters region 1, and only through region 2 if HTO enters region 2. The greater the cross-section area of region 1, the more significant the influence of region 1 on apparent diffusion coefficients and activation energies becomes. In the parallel diffusion model, the ratio of the cross-section area of gel pores to the cross-section area of the total pores is equal to the ratio of gel porosity to total porosity. In both of the cases of the serial model and the parallel model, the ratio of the volume of region 1 to the total pore volume (n), which is the same as the ratio of gel porosity to total porosity, is an important parameter determining the significance of

region 1.

The conceptual diagram illustrated in **Figure 2-8** can be simplified as shown in **Figure 2-9** using the volume ratio (n). The simplified models presented in **Figure 2-9** were fitted to the experimental results obtained in this study using the volume ratio (n) as one of the parameters. In the simplified serial model (**Figure 2-9 (a)**), the apparent diffusion coefficient of HTO can be expressed as

$$\frac{1}{D_a} = \frac{n}{D_a^{R1}} + \frac{1-n}{D_a^{R2}}, \tag{2-11}$$

where D_a^{R1} and D_a^{R2} are apparent diffusion coefficient of region 1 and region 2, respectively. Similarly, in the simplified parallel model (**Figure 2-9 (b)**), the apparent diffusion coefficient is

$$D_a = n \cdot D_a^{R1} + (1-n) \cdot D_a^{R2}. \tag{2-12}$$

The apparent diffusion coefficients of region 1 and region 2 as a function of temperature are respectively expressed by the following equations;

$$D_a^{R1} = \frac{D_v^{R1}}{F.F.} \exp\left[\frac{E_a^{R1}}{R}\left(\frac{1}{298} - \frac{1}{T}\right)\right] \tag{2-13}$$

and

$$D_a^{R2} = \frac{D_v^{R2}}{F.F.} \exp\left[\frac{E_a^{R2}}{R}\left(\frac{1}{298} - \frac{1}{T}\right)\right], \tag{2-14}$$

where D_v^{R1} and D_v^{R2} are diffusion coefficient of water in region 1 and region 2, respectively, E_a^{R1} and E_a^{R2} are activation energy of diffusion for water molecules in region 1 and region 2, respectively, and $F.F.$ is formation factor of the diffusion pathways. The formation factor of diffusion pathways of region 1 and region 2 are

assumed to equal in both of the diffusion models. The values of D_v^{R1} and E_a^{R1} are assumed to be the values in supercooled bulk water (1.6×10^{-10} m^2 s^{-1} and 44.4 kJ mol^{-1}, respectively [18]). The values in bulk liquid water (2.4×10^{-9} m^2 s^{-1} and 19.2 kJ mol^{-1}, respectively [17]) are used as the D_v^{R2} and E_a^{R2} values. The values of n and $F.F.$ at each w/c ratio are parameters determined by the least-squares fitting of Equations (2-11) and (2-12) to apparent diffusion coefficients obtained in the experiment in this study. In all of the cases of the w/c ratio and temperature, the apparent diffusion coefficients were well reproduced by Equations (2-11) and (2-12) as shown in **Figure 2-10**; these fitting curves were close to Arrhenius equation in the temperature range from 293 to 323 K. The optimum values of n and $F.F.$ obtained by fitting are given in **Table 2-4**.

In the serial model, the optimum values of n increased from 0.010 to 0.076 with the decrease in w/c ratio from 0.60 to 0.36. The increase in the activation energies with the decrease in w/c ratio observed in the experiment corresponded to a small increase of a few percent in the volume ratio of region 1 to the total pore volume (n). The values of n obtained from the optimization were small ranging from 1 to 7.6 % of the total pore volume, indicating that diffusion pathways in HCP consist of mostly region 2, and the contribution of region 1 is very small. It should be also noted that the values of n are much smaller than the experimentally determined ratio of gel porosity to total porosity (0.594, 0.416, 0.274 at the w/c ratio of 0.36, 0.45, 0.60, respectively). This means that only a very small part of gel pores contributes to diffusion of HTO in HCP. Most of the gel pores, which can be experimentally determined by, e.g., measuring weight loss after drying, do not participate as diffusion pathways. The optimum values

of $F.F.$ decreased from 75.7 to 25.7 with the increase in w/c ratio. Capillary pores are known to develop with an increase in w/c ratio, and this decrease in $F.F.$ may indicate significance of retardation effect of pore geometry (tortuosity and constrictivity) on HTO diffusion in HCP as w/c ratio decreases.

The small values of n indicate that capillary pores (region 2) are dominant diffusion pathways with very small part (1 to 8 percent) consisting of gel pores (region 1) connected in series in the direction of diffusion. This may be viewed as a pore network mostly consisting of capillary pores, which has some very narrow pores that are plugged with hydrates. In these hydrates, HTO must diffuse through gel pores. In other words, only the gel pores that plug the capillary pore network participate as diffusion pathway. This structure of diffusion pathway is consistent with the n values which are significantly smaller than the experimentally determined ratio of the gel pore volume to the total pore volume. Gel pores that exist outside the capillary pore network, or that exist in the capillary pore network without plugging them do not significantly contribute as diffusion pathways. This view of HCP microstructure presented from the serial model optimization results may be reasonable together with the changes in n and $F.F.$ values indicating the increasing significance of gel pores and pore geometry as w/c ratio decreases.

In contrast, the parameters n and $F.F.$ obtained from the parallel model were not in a practical range. The n values increased from 0.461 to 0.912 with the decrease in w/c ratio. These n values are much greater than the experimentally determined ratio of gel porosity to total porosity, and are not reasonable even when a 1.0 nm layer of confined water on the inner-surfaces of the capillary pores is taken into

consideration. In addition, the values of $F.F.$ were almost constant at 22.4 ± 4.8. This result indicates that there is no change in pore geometry with the changes in w/c ratio, which contradicts with the concept that microstructure of HCP depends on the w/c ratio [12]. Although the experimental data was fitted well with the parallel model by optimizing n and $F.F.$, both parameters did not reflect the microstructure of HCP, suggesting that the parallel model possibly failed to express the relationship between diffusion and the microstructure of HCP.

Between the two basic modules considered as diffusion pathway models in HCP, the serial model represents a more realistic pore network. In the serial model, capillary pores (region 2) are the dominant diffusion pathway, and only some percent of the diffusive pore volume comprised gel pores (region 1). Previous studies [5, 6] focusing on the relationship between porosity and diffusivity in HCP may have failed to emphasize the significance of gel pores because the contribution of gel pores to diffusivity is, in general, relatively small. With the same reason, a simple expression of the relationship between the diffusion coefficient and capillary porosity, such as Archie's law seemed to be valid.

The activation energy obtained in this study through systematically examining the temperature dependence of diffusion coefficient enabled us to identify the effect of region 1, which does not contribute significantly to the diffusion coefficient, but does affect the activation energy. The same approach can be easily applied to study diffusion of different chemical species in cementitious materials, or diffusion in cement pastes of different composition including aggregates and admixtures. Further investigations can reveal how the microstructure affects diffusion coefficient, which will lead to a better

assessment of the performance of cementitious materials as an engineered barrier in radioactive waste disposal.

Table 2-2 Water contents, hydration degree, and porosity of HCP samples.

w/c ratio [-]	Weight		Hydration degree	Total porosity	Capillary porosity	Gel porosity	Effective porosity
	Porewater m_p [g]	Bound-water m_c [g]	α [-]	ε_{tot} [-]	ε_{cap} [-]	ε_{gel} [-]	ε_{eff} [-]
0.36	0.694	0.543	0.77	0.29	0.12	0.17	0.32
0.40	0.752	n.d.*	—	0.31	—	—	0.30
0.45	0.845	0.583	0.83	0.35	0.21	0.14	0.33
0.50	0.923	0.581	0.83	0.38	0.25	0.13	0.35
0.60	1.036	0.618	0.88	0.44	0.31	0.13	0.41

* : not determined

Table 2-3 **Apparent diffusion coefficient (D_a) of HTO and $H_2{}^{18}O$ and activation energy (E_a) of HTO in HCP. Abbreviations of Ins. and Cons. are instantaneous source and constant source, respectively.**

Tracer	Method	w/c ratio	D_a [$\times 10^{-11}$ m^2/s]				E_a
		[-]	293 K	303K	313 K	323 K	[kJ mol^{-1}]
HTO	Ins.	0.36	1.1	2.0	2.7	4.3	31.3±2.7
			1.3	1.9	2.6	3.9	
		0.45	2.8	4.2	5.9	7.1	22.9±1.3
			2.8	4.3	5.8	7.6	
		0.60	6.2	9.9	13.0	16.0	21.5±3.1
			7.7	9.9	13.0	17.0	
	Con.	0.36	—	2.6	—	—	—
		0.45	—	4.0	—	—	—
		0.60	—	9.2	—	—	—
$H_2{}^{18}O$	Con.	0.40	—	2.6	—	—	—
		0.45	—	3.7	—	—	—
			—	3.3	—	—	—
		0.50	—	4.2	—	—	—
		0.60	—	7.6	—	—	—

Table 2-4 **The model optimization results. The values of *n* (the volume ratio of region 1 to diffusion pathways) and formation factor of the diffusion pathways (*F.F.*) for the serial model and the parallel model were obtained by fitting the experimental data to the models.**

w/c ratio	Serial model		Parallel model	
[-]	*n*	*F.F.*	*n*	*F.F.*
0.36	0.076	75.7±13.7	0.912	23.5±4.4
0.45	0.015	56.8±3.3	0.649	27.2±5.9
0.60	0.010	25.7±3.3	0.461	16.6±11.7

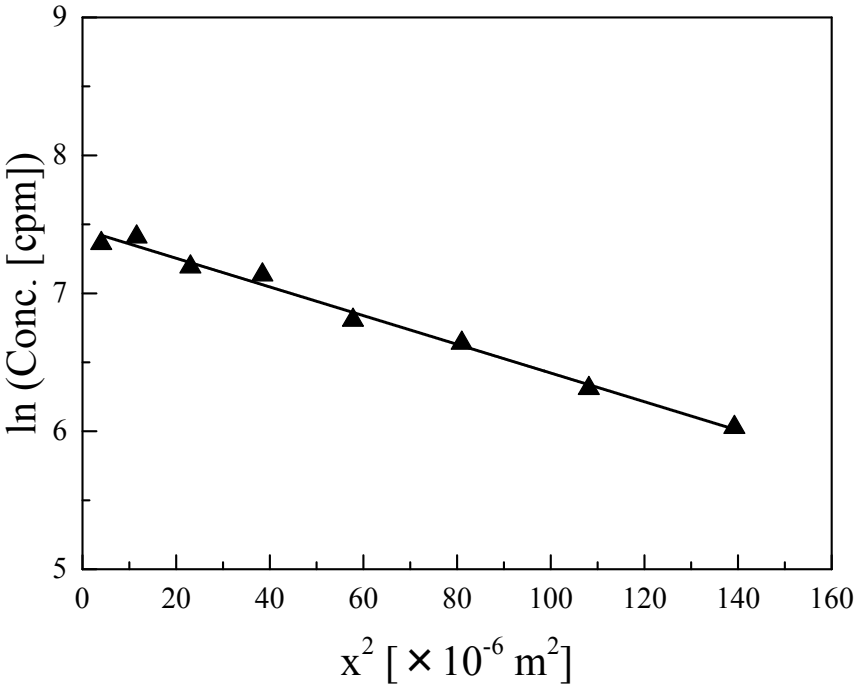

Figure 2-2 **Concentration profile of HTO in HCP at w/c ratio of 0.45 at 303 K for an instantaneous source; diffusion period was 7days. A solid line is a fitting curve by solution of Fick's second law (Equation (2-7)).**

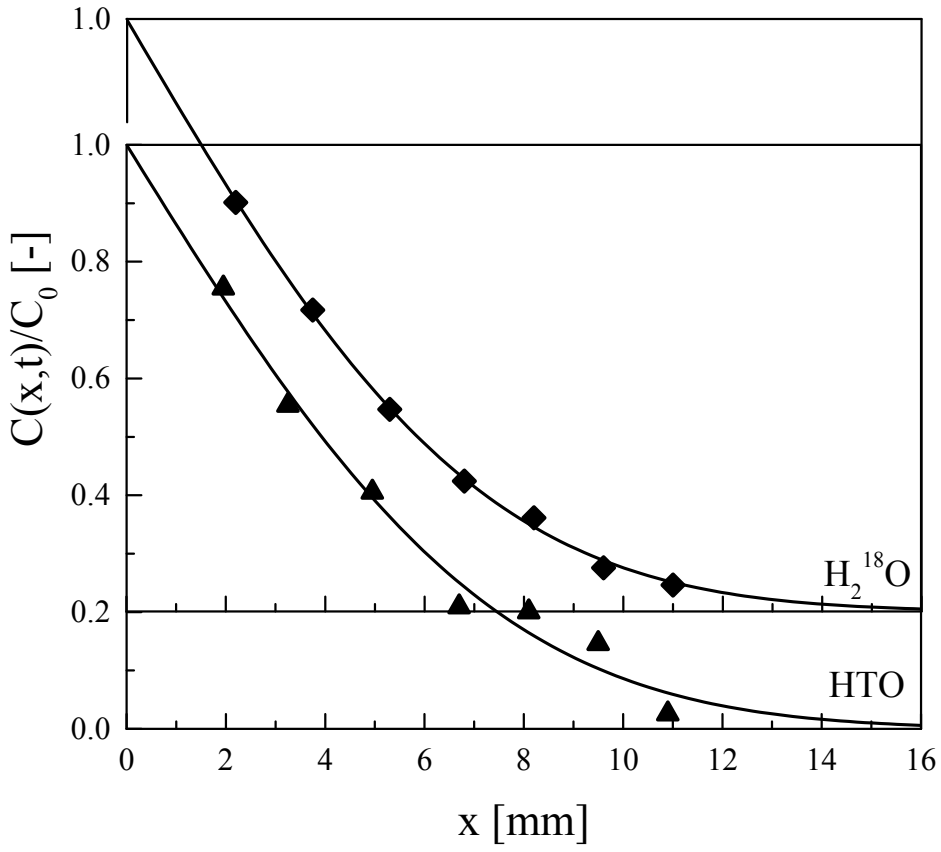

Figure 2-3 **Concentration profiles of HTO and $H_2{}^{18}O$ in HCP at w/c ratio of 0.45 at 303 K for a constant source; diffusion period was 5days. A solid line is a fitting curve by solution of Fick's second law (Equation (2-8)).**

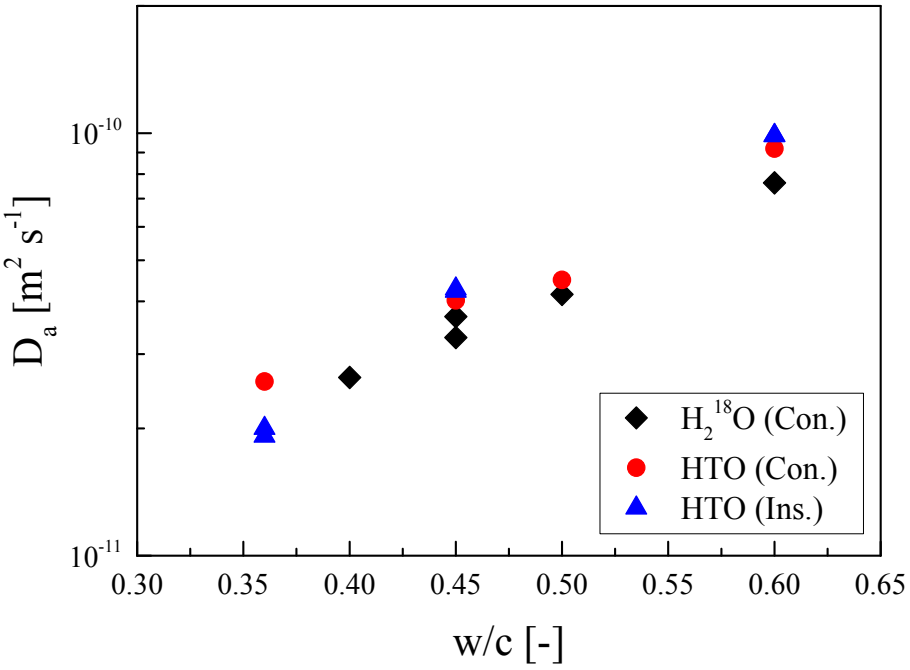

Figure 2-4 **Dependence of apparent diffusion coefficients of HTO and $H_2{}^{18}O$ on w/c ratio (at 303 K). Abbreviations of Ins. and Cons. are instantaneous source and constant source, respectively.**

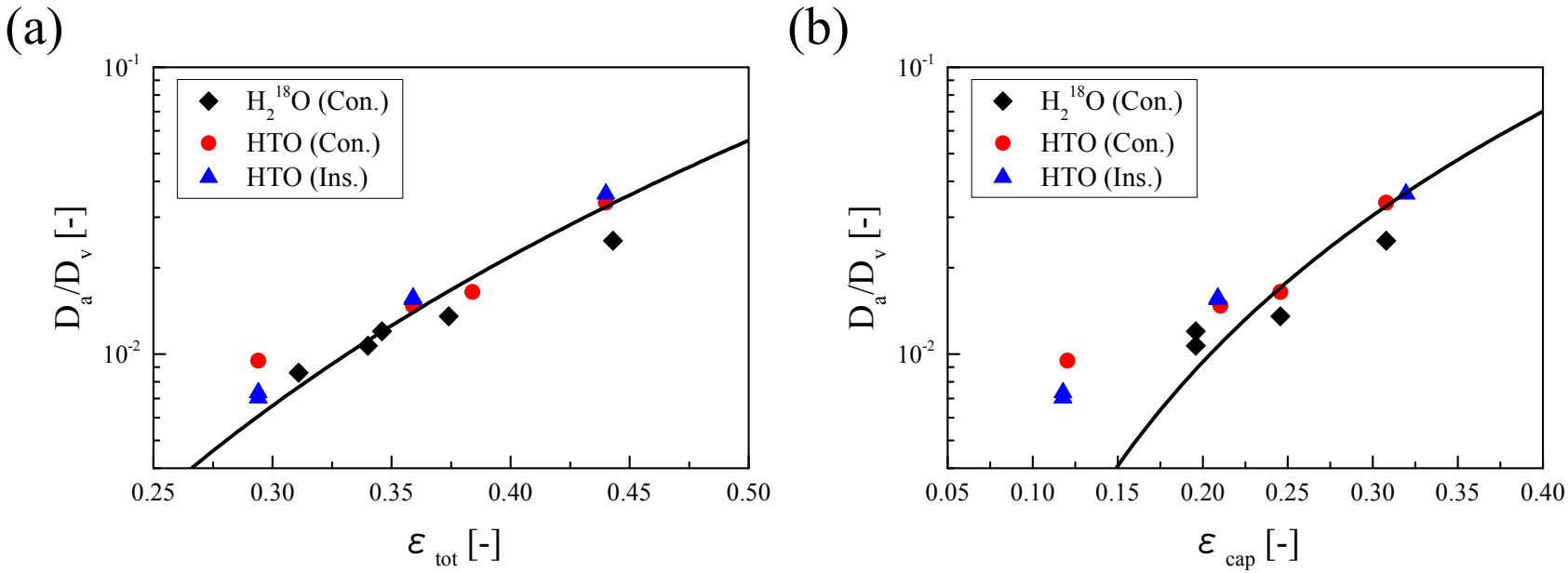

Figure 2-5 **Relationship between the porosity and the apparent diffusion coefficients of $H_2{}^{18}O$ and HTO; (a) total porosity, (b) capillary porosity. Abbreviations of Ins. and Cons. are instantaneous source and constant source, respectively. Solid line shows the best fit as a power function of porosity.**

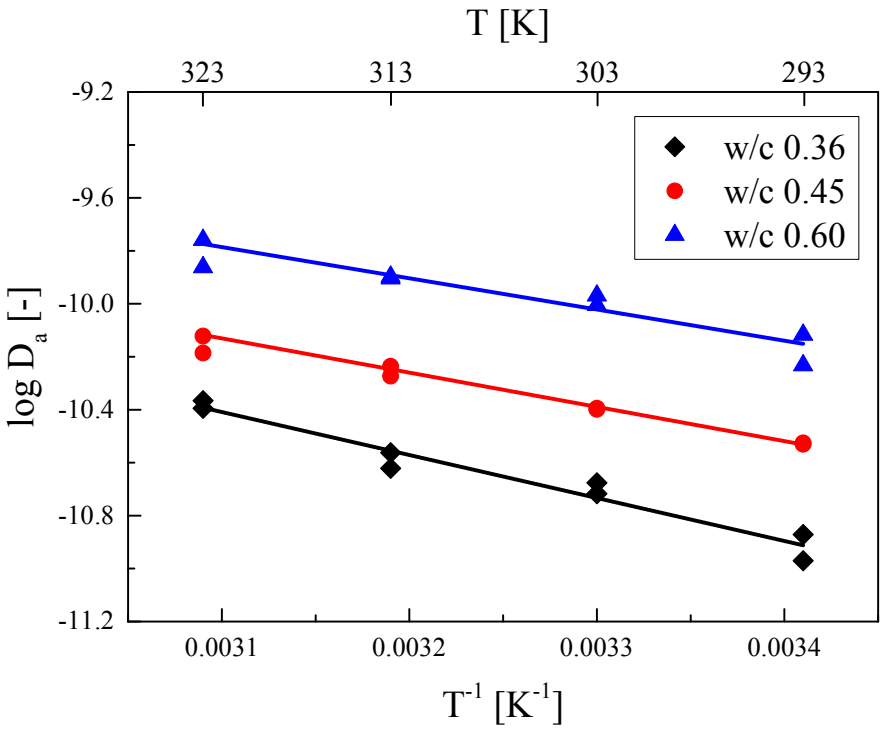

Figure 2-6 Arrhenius plots of the apparent diffusion coefficients of HTO in HCP at w/c ratio of 0.36, 0.45, and 0.60.

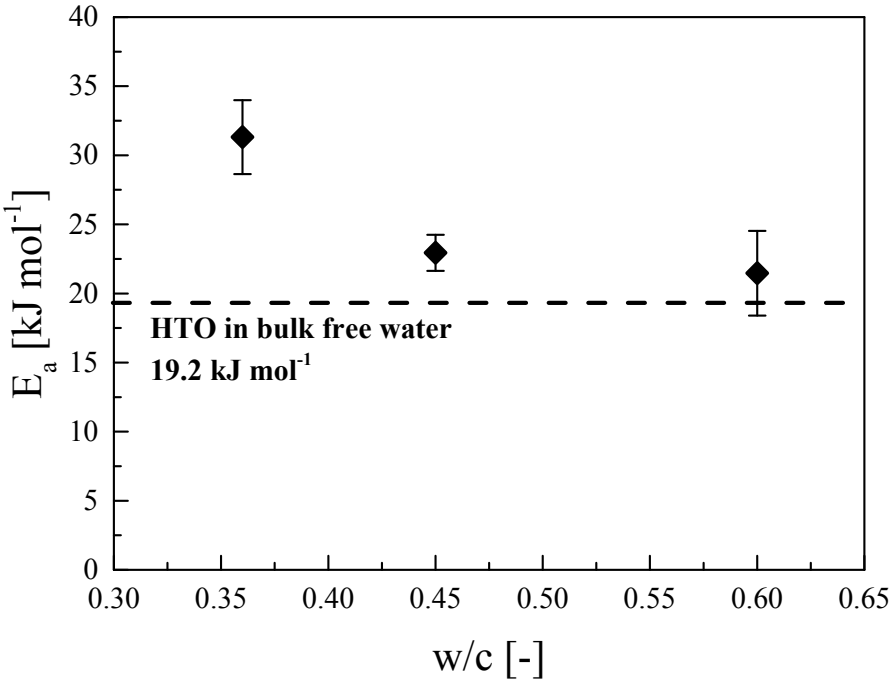

Figure 2-7 **Dependence of activation energies of HTO diffusion in HCP on w/c ratio. Dashed line indicates the activation energy of diffusion for HTO in bulk liquid water (19.2 kJ mol^{-1} [17]).**

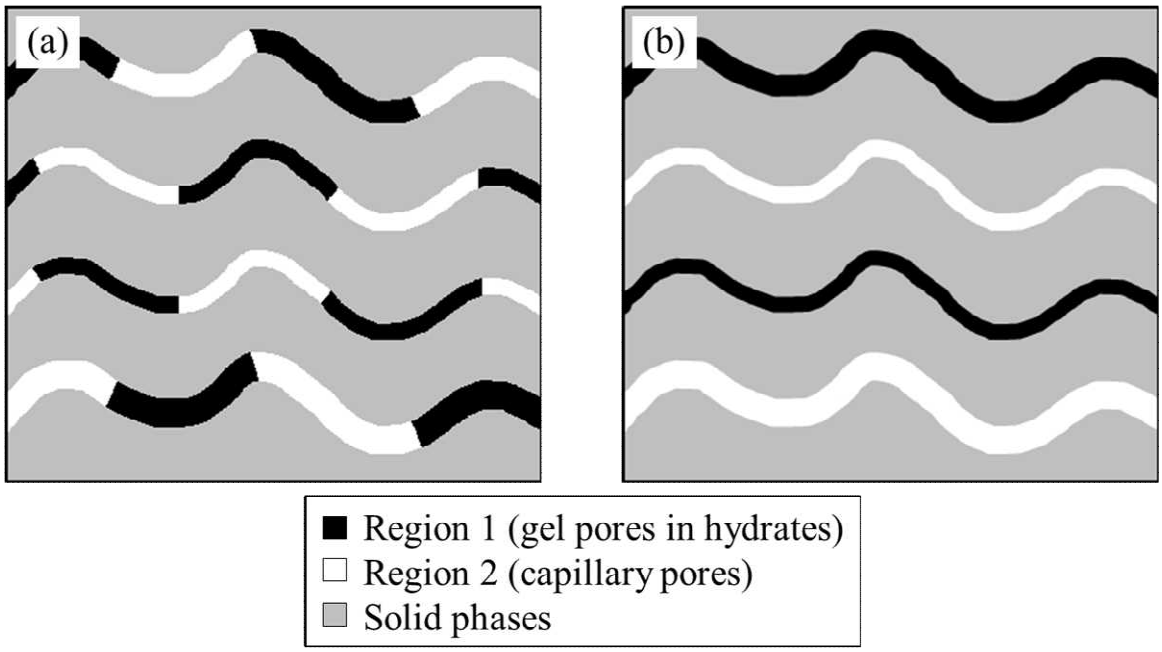

Figure 2-8 **Schematic diagrams of the microstructure of HCP: (a) the serial model, (b) the parallel model. Black parts are hydrates including gel pores (region 1), white parts are capillary pores (region 2), and gray parts are solid phases such as hydrates and unhydrated cements.**

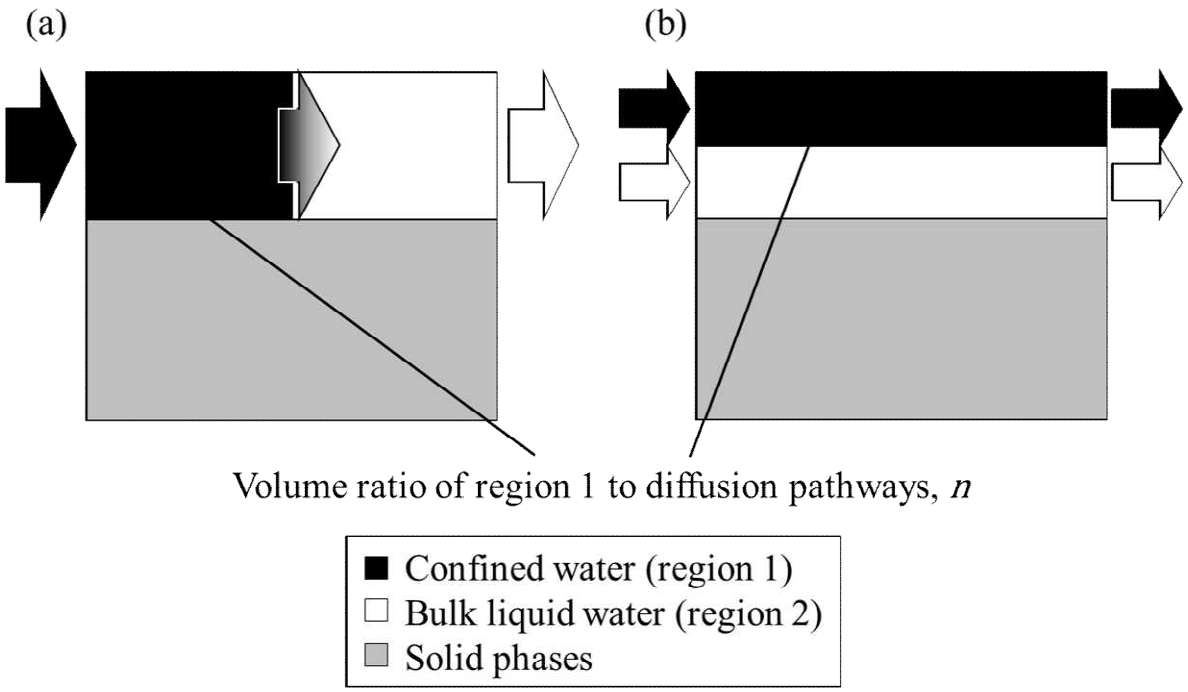

Figure 2-9 **Schematic diagrams of the simplified models shown in Figure 2-8: (a) the serial diffusion model, (b) the parallel diffusion model. The arrows indicate the direction of HTO diffusion through the model.**

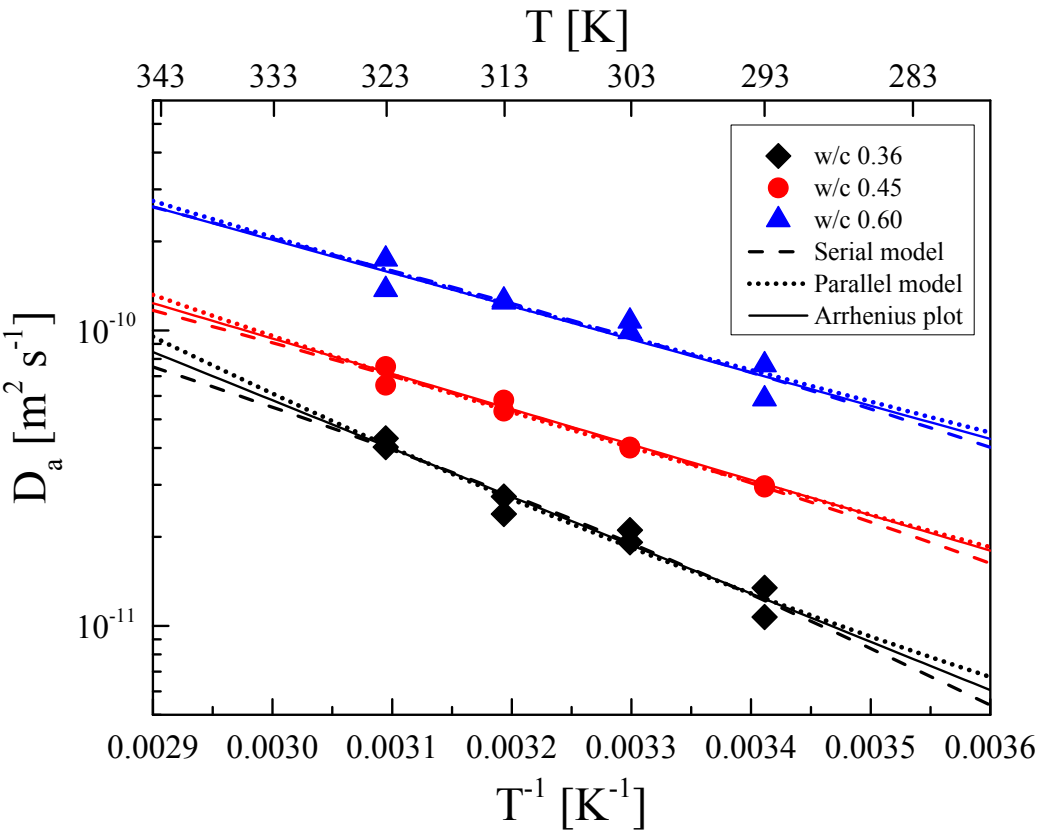

Figure 2-10 **Model optimization results with experimental data. Apparent diffusion coefficients of HTO are shown as a function of w/c ratio. Dashed line shows the results of the serial diffusion model and the dotted line shows the parallel diffusion model.**

2.4 Conclusions

In order to study the diffusion of water in HCP, the non-steady diffusion experiments were conducted using HTO and $H_2{}^{18}O$ as tracers using HCP samples prepared at w/c ratio from 0.36 to 0.60, and at different temperatures (293 to 323 K). The values of D_a ranged from 1.1×10^{-11} m^2 s^{-1} to 1.7×10^{-10} m^2 s^{-1}, and increased with increasing w/c ratio. The D_a values for $H_2{}^{18}O$ ranged from 2.6×10^{-11} m^2 s^{-1} to 7.6×10^{-11} m^2 s^{-1} at w/c ratio from 0.40 to 0.60 at diffusion temperature of 303 K. The values of D_a for $H_2{}^{18}O$ were in good agreement with those for HTO at each w/c ratio, suggesting that both HTO and $H_2{}^{18}O$ diffused as H_2O molecule and dissociation of water molecule is negligible in diffusion even at high pH in HCP.

The values of E_a of HTO at w/c ratio of 0.36, 0.45, and 0.60 were 31.3 kJ mol^{-1}, 22.9 kJ mol^{-1}, and 21.5 kJ mol^{-1}, respectively. The higher activation energy of 31.3 kJ mol^{-1} than in bulk liquid water (19.2 kJ mol^{-1}) was observed at w/c ratio of 0.36. Water in gel pores may be confined by hydrates to form a diffusion regime with higher E_a, such as supercooled bulk water, and the contribution of this regime may become significant in a whole HCP at low w/c ratio. Based on the microstructure of HCP, simple diffusion models were considered that consist of a region of bulk liquid water (capillary pores) and a region of water confined by hydrates (gel pores). The models were fit with the D_a values experimentally obtained in this study. From the model results, dominant diffusion pathway of water in HCP was that capillary pores and gel pores arranged in series in the direction of diffusion, and the pathway mostly consists of capillary pores. The ratio of gel pores contributing to diffusion was significantly smaller than the ratio of gel porosity to total porosity determined by the experiment, indicating that a very

small part of gel pores that plug capillary pores may participate in diffusion and most of gel pores may not function as diffusion pathways. The activation energy obtained in this study enabled us to identify the influence of gel pores, which may be filled with water confined by hydrates, on diffusion of HTO in HCP. This approach of examining the activation energy of diffusion may also be applicable for other chemical species, and other types of cementitious materials.

References

[1] Japan Nuclear Cycle Development Institute and Federation of Electric Power Companies, JNC-TY1400 2005-001(1)/FEPC TRU-TR2-2005-03 in Japanese.

[2] Fujisaki K., Kubota S., Ueda H., Yamamoto T., Sugiyama D., Chida T., *Investigation of the methodology for selecting cementitious materials for the different components in the underground facility - Deriving component requirements and investigation of the weighting methodology*, Nuclear Waste Management Organization of Japan, NUMO-TR-13-07, 14-30 (2014).

[3] Delagrave A., Marchand J., Pigeon M., "Influence of Microstructure on the Tritiated Water Diffusivity of Mortars," *Advn. Cem. Bas. Mat.*, **7**, 60-65 (1998).

[4] Revertegat E., Richet C., Gégout P., "Effect of pH on the durability of cement pastes," *Cem. Concr. Res.*, **22**, 259-272 (1992).

[5] Numata S., Amano H., Minami K., **"**Diffusion of tritiated water in cement materials," *J. Nucl. Mat.*, **171**, 373-380 (1990)

[6] Yamaguchi T., Negishi K., Hoshino S., Tanaka T., "Modeling of diffusive mass transport in micropores in cement based materials," *Cem. Concr. Res.*, **39**, 1149-1155 (2009).

[7] Bejaoui S., Bary B., "Modeling of the link between microstructure and effective diffusivity of cement pastes using a simplified composite model," *Cem. Concr. Res.*, **37**, 469-480 (2007).

[8] Kamali-Bernard S., Bernard F., Prince W., "Computer modelling of tritiated water diffusion test for cement based materials," *Comp. Mat. Sci.*, **45**, 528-535 (2009).

[9] Gallé C., “Effect of drying on cement-based materials pore structure as indentified by mercury intrusion porosimetry – A comparative study between oven-, vacuum-, and freeze-drying,” *Cem. Concr. Res.*, **31**, 1467-1477 (2001).

[10] Cook R. A., Hover K. C., “Mercury porosimetry of hardened cement pastes,” *Cem. Concr. Res.*, **29**, 933-943 (1999).

[11] Lam L., Wong Y. L., Poon C. S., “Degree of hydration and gel/space ratio of high-volume fly ash/cement systems,” *Cem. Concr. Res.*, **30**, 747-756 (2000).

[12] Mindess S., Young J. F., Darwin D., *Concrete 2nd ed.*, Prentice Hall, Pearson Education Inc., Upper Saddle River, New Jersey, 57-91 (2003).

[13] Tanaka S., Noda N., Higashihara T., Sato S., Kozaki T., Sato H., Hatanaka K., “Kinetic behavior of water as migration media in compacted montmorillonite using $H_2{}^{18}O$ and applying electric potential gradient,” *Phys. Chem. Earth.*, **33**, S163-S168 (2008).

[14] Igarashi S., Kawamura M., Watanabe A., “Analysis of cement pastes and mortars by a combination of backscatter-based SEM image analysis and calculations based on the Powers model,” *Cem. Concr. Compos.*, **26**, 977-985 (2004).

[15] Wong H. S., Buenfeld N. R., “Determining the water-cement ratio, cement content, water content and degree of hydration of hardened cement paste: Method development and validation on paste samples,” *Cem. Concr. Res.*, **39**, 957-965 (2009).

[16] Crank J., *The Mathematics of Diffusion 2nd ed.*, Clarendon Press, Oxford, 11-27 (1975).

[17] Wang J. H., Robinson C. V., Edelman I. S., "Self-diffusion and Structure of Liquid Water. III. Measurement of the Self-diffusion of Liquid Water with H^2, H^3 and O^{18} as Tracers," *J. Am. Chem. Soc.*, **75**, 466-470 (1953).

[18] Price W. S., Hiroyuki I., Yoji A., "Self-Diffusion of Supercooled Water to 238 K Using PGSE NMR Diffusion Measurements," *J. Phys. Chem. A*, **103**, 448-450 (1999).

[19] Fratini E., Faranoe A., Baglioni P., Bellissent-Funel M.-C., Chen S.-H., "Dynamic scaling of QENS spectra of glassy water in aging cement paste," *Phys. A*, **304**, 1-10 (2002).

[20] Fratini E., Chen S.-H., Baglioni P., Bellissent-Funel M.-C., "Quasi-Elastic Neutron Scattering Study of Translational Dynamics of Hydration Water in Tricalcium Silicate," *J. Phys. Chem. B*, **106,** 158-166 (2002).

[21] Youssef M., Pellenq R. J.-M., Yildiz B., "Glassy Nature of Water in an Ultraconfining Disordered Material: The Case of Calcium-Silicate-Hydrate," *J. Am. Chem. Soc.*, **133**, 2499-2510 (2011).

[22] Garboczi E. J., Bentz D. P., "Computer simulation of the diffusivity of cement-based materials," *J. Mater. Sci.*, **27**, 2083-2092 (1992).

Chapter 3
Water-to-cement ratio dependence of diffusion behavior of Na^+ and Cs^+ ions in hardened cement pastes

3.1 Introduction

Leaching of alkaline components (NaOH, KOH, and $Ca(OH)_2$) from cement-based materials may cause deterioration of the barrier performance of not only cement-based materials used in low level radioactive waste (LLW) disposal, but also other barrier materials (i.e. bentonite and geological features) used both in LLW and high level radioactive waste (HLW) disposal [1, 2]. Ionic diffusion can be influenced by interactions between ions and cement hydrates in addition to pore geometry. Previous studies [3-5] suggested that the chemical or electrochemical characteristics of the surface of cement hydrates influenced ionic diffusion. However, interactions between ions and cement hydrates are still unclear and the detailed ionic diffusion mechanism is controversial. Reliable safety assessment of disposal for LLW and HLW requires the understanding of diffusion mechanisms of chemical species with positive charges in cement-based materials including the relationship between the microstructure and interactions with the surfaces.

A simple model consisting of capillary and gel pores was proposed in Chapter 2 to estimate the degree of contribution of gel pores in diffusion of HTO in HCP from the analysis of the activation energy for diffusion assuming that gel pores are filled with water similar to supercooled bulk water. A serial model, in which capillary and gel pores are arranged in series in the direction of diffusion, fit the data well with parameters

within a reasonable range, suggesting that the diffusion pathway of water in HCP mostly consists of capillary pores. The ratio of gel pores contributing to diffusion was significantly smaller than the ratio of gel porosity to total porosity determined by the experiment, indicating that a very small part of gel pores that plug capillary pores participate in diffusion and most of gel pores do not function as diffusion pathways. Similar analysis of charged ions may allow us to elucidate the diffusion behavior of ions in HCP.

In this Chapter, the diffusion behavior of alkali metal ions (sodium and cesium) in HCP was examined. Understanding the diffusion behavior of sodium ion, which is not only a representative monovalent cation but also the cation from a cement alkaline component (NaOH), is very important in the assessment of a long-term durability and barrier performance of cement-based materials and the influence of high alkaline solution on other barrier materials (bentonite and geological features). Understanding the diffusion behavior of cesium ion, which is contained in radioactive waste as a major fission product (Cs-135 and Cs-137), is essential in assessing the safety of radioactive waste disposal, because cesium ion can easily dissolve and migrate in groundwater in comparison to other radionuclides, and Cs-135 has a long half-life of 2.3×10^6 years. The apparent diffusion coefficients for Na^+ and Cs^+ ions in HCP prepared at different w/c ratio were determined using Na-22 and Cs-137 as tracers by a non-steady diffusion method at diffusion temperature from 293 to 323 K. In addition, the sorption of Na^+ and Cs^+ ions on HCP was examined by batch sorption experiments. Based on the temperature dependence of the apparent diffusion coefficients, activation energies for diffusion were determined at each w/c ratio examined. Considering the sorption of Na^+

and Cs^+ on HCP, the mechanisms of diffusion processes for Na^+ and Cs^+ ions in HCP was discussed using the model developed for HTO diffusion in HCP in Chapter 2.

3.2 Experimental methods

3.2.1 Preparation of HCP samples

The HCP samples with w/c ratio of 0.36, 0.45, and 0.60 were prepared and characterized by the same method described in Section 2.2.1 and 2.2.2, respectively. The degree of hydration (α), total porosity (ε_{tot}), capillary porosity (ε_{cap}), and gel porosity (ε_{gel}) for each HCP sample used in sorption and diffusion experiments for Na^+ and Cs^+ ions are shown in **Table 3-1**.

3.2.2 Batch sorption

Distribution coefficients of Na^+ and Cs^+ ions were determined by the batch sorption method for the HCP samples with different w/c ratios of 0.36, 0.45, and 0.60. The HCP samples were dried in an oven at 333 K for more than 1 week, ground to powder with mortar and pestle, and sieved to obtain fine particles with diameter less than 75 μm. The sorption experiments were conducted with 0.1000±0.010 g of the fine particles and 10 ml of cement-equilibrated water (the solid/liquid ratio = 100) in 15-ml centrifuge tubes, which were agitated for more than 1 day to attain an equilibrium between solid and liquid phase. The concentrations of Na, K, Ca, Si, Al, and Fe in the cement-equilibrated water were determined with ICP-AES (ICP-9000, SHIMADZU, Ltd.), and are listed in **Table 3-2**. After equilibrating, 20μl of either NaCl solution containing 800 Bq of Na-22, or CsCl solution containing 740 Bq of Cs-137 was introduced into the centrifuge tube, which was continuously mixed for a designated period of time at a prescribed temperature. **Table 3-3** lists the experimental conditions including the concentrations of Na^+ and Cs^+ ions in the liquid phase, the sorption time,

and the sorption temperature. After the sorption, the liquid phase was separated by centrifugation at 4800 rpm for 30 minutes (05PR-22 centrifuge, Hitachi, Ltd.), and filtrated with a hydrophilic polytetrafluoroethylene (PTFE) type membrane filter with 0.45 μm pore size (25HP045AN, ADVANTEC). The radioactivity of Na-22 or Cs-137 in the filtrate was determined with a well-type NaI(Tl) scintillation detector (AccuFLEXγ7000, Aloka, Ltd.). The batch sorption experiment was conducted in triplicate for each experimental condition, in addition to a blank test which was conducted without solid phase to check the sorption of the tracers on the inner wall of the centrifuge tube. The radiotracers of Na-22 (PerkinElmer. Inc.) and Cs-137 (Eckert & Ziegler Isotope Products Inc.) were obtained from Japan Radioisotope Association (JRIA).

3.2.3 Non-steady diffusion method

The apparent diffusion coefficients (D_a) of Na^+ and Cs^+ ions in the HCP samples with different w/c ratios were determined by a non-steady diffusion method with an instantaneous source (Na-22 or Cs-137), as described in Section 2.2.3. The tracer solutions spiked to the HCP sample were 4×10^{-6} M NaCl containing 400 kBq of Na-22 and 2×10^{-6} M CsCl containing 370 kBq of Cs-137. After the diffusion, in order to determine the concentration profile, the HCP sample was powdered with emery paper into sections of 0.15-0.5 mm thickness in the direction of diffusion from the side on which the radiotracer was spiked. The radioactivity of Na-22 or Cs-137 of the powdered HCP specimen was determined with an NaI scintillation counter (AccuFLEXγ7000, Aloka, Ltd.).

Table 3-1 **Degree of hydration (α), total porosity (ε_{tot}), capillary porosity (ε_{cap}), and gel porosity (ε_{gel}) for HCP used in the experiments. At w/c ratio of 0.36, HCP samples used for Na^+ ion and Cs^+ ion experiments were different.**

w/c ratio [-]	Nuclide	Hydration degree α [-]	Total porosity ε_{tot} [-]	Capillary porosity ε_{cap} [-]	Gel porosity ε_{gel} [-]
0.36	Na	0.713	0.288	0.152	0.136
	Cs	0.722	0.295	0.147	0.148
0.45	Na, Cs	0.777	0.357	0.221	0.136
0.60	Na, Cs	0.809	0.432	0.335	0.097

Table 3-2 Components of the cement-equilibrated water.

Element	Concentration [mM]
Na	4.3
K	20.0
Ca	52.1
Si	< 1
Al	n.d.*
Fe	n.d.*

*: not detected

Table 3-3 Conditions of the batch sorption experiment.

w/c ratio [-]	Particle size [μm]	Solid:Liquid ratio [-]	Concentrations of Na^+ and Cs^+ [mM]	Sorption period [days]	Temperature [K]
0.36	<75	1:100	10^{-3}, 5×10^{-3}, 5×10^{-2}, 10^{-1}	14	303
			10^{-2}	3, 5, 7, 21	303
			10^{-2}	14	293, 303, 313, 323
0.45, 0.60	<75	1:100	10^{-2}	14	303

3.3 Results and discussion

3.3.1 Sorption of Na^+ ion and Cs^+ ion on HCP

No change in the radiotracer concentration in the liquid phase was detected in the blank tests, indicating sorption of the tracer on the inner wall of the centrifugation tube was negligible. Therefore, the apparent distribution coefficient, K_d, can be determined from the batch experiment initial concentration (C_0) and the equilibrated concentration (C_{eq}) of the radiotracer in the liquid phase by using the following equation:

$$K_d = \frac{C_0 - C_{eq}}{C_{eq}} \cdot \frac{V}{M}, \tag{3-1}$$

where V is the volume of liquid phase (ml) and M is the weight of solid phase (g).

In the sorption experiment, however, the radiotracer concentration at equilibrium in the liquid phase was the same as the initial concentration (i.e. $C_0 = C_{eq}$), indicating that neither Na-22 nor Cs-137 sorb on the HCP (i.e. $K_d = 0$) under the experimental conditions in this study. This seems to be inconsistent with the previous studies reporting the sorption of Na^+ ion [6] and Cs^+ ion [7] on a synthesized calcium-silicate-hydrate (C-S-H), which is a major hydrate of the HCP. However, this discrepancy can be attributed to the orders of magnitude higher concentrations of the tracers used in the previous study (Na^+:0.1-300 mM, Cs^+: 500 mM) than those in this study (Na^+, Cs^+: 10^{-3} – 10^{-1} mM).

3.3.2 Diffusion coefficients of Na^+ ion and Cs^+ ion

Figure 3-1 and **Figure 3-2** show typical concentration profiles of Na-22 and

Cs-137 in HCP obtained in the instantaneous-source diffusion experiment, respectively. A good linearity was obtained in all cases of w/c ratio and temperature when the logarithm of the tracer concentration was plotted as a function of x^2. The apparent diffusion coefficients (D_a) of Na^+ and Cs^+ ions in HCP were determined by using Equation (2-7) as described in section 2.3.2, and are listed in **Table 3-4**. The D_a values of Na^+ and Cs^+ ions ranged from 5.0×10^{-12} m^2 s^{-1} to 6.0×10^{-11} m^2 s^{-1} and from 5.7×10^{-12} m^2 s^{-1} to 1.0×10^{-10} m^2 s^{-1}, respectively, at w/c ratios ranging from 0.36 to 0.60 and at diffusion temperatures between 293 and 323 K.

Figure 3-3 shows the D_a values of Na^+ and Cs^+ ions at 303 K as a function of w/c ratio, together with those of HTO obtained in Chapter 2 by the same experimental method. The D_a values of Na^+ and Cs^+ ions increased with an increase in w/c ratio similar to the HTO results. The values of D_a decreased in the order of HTO > Cs^+ > Na^+. This order corresponds to the order of their diffusivities in bulk liquid water, i.e. 2.4×10^{-9} m^2 s^{-1} for HTO [8], 1.35×10^{-9} m^2 s^{-1} for Na^+ ion [9], and 2.11×10^{-9} m^2 s^{-1} for Cs^+ ion [9].

3.3.3 Activation energies for the diffusion of Na^+ ion and Cs^+ ion

Arrhenius plots of the D_a values of Na^+ and Cs^+ ions in HCP at different w/c ratio are shown in **Figure 3-4** and **Figure 3-5**, respectively, together with regression lines determined by the least-squares method. A good linearity was identified for the D_a values of Na^+ and Cs^+ ions at each w/c ratio, suggesting the diffusion is dominated by a single process which can be described by the Arrhenius equation, i.e. Equation (2-10) in Chapter 2. The E_a values obtained for Na^+ and Cs^+ ions are listed in **Table**

3-4. The E_a values for Na^+ and Cs^+ ions increased with a decrease in w/c ratio similar to the results of HTO.

3.3.4 Diffusion mechanism of Na^+ ion and Cs^+ ion in HCP

The HCP can be considered to be porous media having capillary and gel pores in it, as discussed in Chapter 2. If the migration of the radiotracer in the HCP is retarded by sorption, the apparent diffusion coefficient (D_a) can be expressed with the distribution coefficient (K_d) by the following equation;

$$D_a = \frac{1}{1+(\rho \cdot K_d)/\varepsilon} \cdot \frac{1}{F.F.} \cdot D_v, \tag{3-2}$$

where D_v is the diffusivity in bulk liquid water, $F.F.$ is the formation factor for the diffusion pathway, ε is the volume ratio of pore available to diffusion, and ρ is the density of a sample. By substituting the Equation (3-2) with the Equation (2-10), the D_a can be expressed by the following equation;

$$D_a = D_a^0 \exp\left(-\frac{E_a}{RT}\right) = \frac{1}{(\rho \cdot K_d^0)/\varepsilon} \cdot D_v^0 \exp\left(-\frac{E_a^{net} - \Delta H}{RT}\right), \tag{3-3}$$

where the superscript of "0" indicates that the diffusivity is an arbitrary constant and E_a^{net} is the net activation energy for diffusion process without sorption, and ΔH is the enthalpy for sorption (kJ mol^{-1}). This means that the E_a value obtained from the temperature dependence of the D_a values contains the contribution of the sorption enthalpy (ΔH);

$$E_a = E_a^{net} - \Delta H. \tag{3-4}$$

The ΔH value can be determined from the temperature dependence of the distribution

coefficients expressed in the Van't Hoff's equation [10];

$$K_d = B' \exp\left(-\frac{\Delta H}{RT}\right), \tag{3-5}$$

where B' is an arbitrary constant, R is the gas constant (8.31 J mol^{-1} K^{-1}), and T is absolute temperature (K).

In this study, however, the sorption enthalpy (ΔH) for Na^+ and Cs^+ ions on the HCP was negligible, since no sorption was identified both for Na^+ and Cs^+ ions on the HCP as mentioned in the section 3.3.1. Therefore, the E_a value for the diffusion of Na^+ and Cs^+ ions in the HCP obtained in this study can represent a predominant diffusion process.

Figure 3-6 shows the w/c ratio dependence of the E_a values of the diffusion of Na^+ and Cs^+ ions in HCP, together with the E_a values of HTO in HCP, and the E_a values of HTO, Na^+ and Cs^+ in bulk water. The E_a values for Na^+ and Cs^+ diffusion in HCP at w/c ratio of 0.60 (Na^+: 14.8 kJ mol^{-1}, Cs^+: 18.7 kJ mol^{-1}) were almost the same as the values in bulk water (Na^+: 18.4 kJ mol^{-1}, Cs^+: 16.4 kJ mol^{-1} [9]), suggesting that the dominant diffusion process at high w/c ratio is similar to diffusion in bulk water. On the other hand, at lower w/c ratio, especially at the w/c ratio of 0.36, the values of E_a were significantly greater than in bulk liquid water (Na^+: 34.1 kJ mol^{-1}, Cs^+: 31.3 kJ mol^{-1}), suggesting that the dominant diffusion process is different. As discussed in Chapter 2, a dominant diffusion pathway of water in the HCP can be the capillary pores with a small volume of gel pores arranged in series in the direction of diffusion. Since Na^+ and Cs^+ ions are highly soluble and do not sorb on the HCP, it is possible that these cations diffuse in the same pathway as HTO, although these cations are hydrated in

water and have larger diameters compared to water molecules.

The same diffusion model proposed in Chapter 2 for HTO, so-called "Serial model" expressed by the equation (2-11), was examined by fitting with the experimental diffusion data obtained for Na^+ and Cs^+ in this study in order to clarify the diffusion mechanism of the cations in the HCP. The D_v^{R2} and E_a^{R2} values of diffusion of Na^+ and Cs^+ ions in bulk water were obtained from literature; 1.35×10^{-9} m^2 s^{-1} and 18.4 kJ mol^{-1} for Na^+ ion, and 2.11×10^{-9} m^2 s^{-1} and 16.4 kJ mol^{-1} for Cs^+ ion [9]. There are no data available, however, for the values of D_v^{R1} and E_a^{R1} for the diffusion of Na^+ and Cs^+ ions in the supercooled bulk water. Therefore, these two values were treated as fitting parameters, while using the values of n and *F.F.* obtained for HTO in Chapter 2 (n: 0.076, *F.F.*: 75.7 at w/c ratio of 0.36, n: 0.015, *F.F.*: 56.8 at w/c ratio of 0.45, and n: 0.010, *F.F.*: 25.7 at w/c ratio of 0.60, as shown in **Table 2-4**).

Figure 3-7 and **Figure 3-8** show the results from the fitting to the experimental data of the D_a for Na^+ and Cs^+ ions, respectively. The fitting curve at each w/c ratio mostly reproduced the experimental data of the D_a for Na^+ and Cs^+ ions. Small discrepancies were observed between the fitting curve and the experimental data at high temperature and high w/c ratio in both cases of Na^+ and Cs^+ ions. The D_v^{R1} and E_a^{R1} values obtained from the fitting were 4.6×10^{-11} m^2 s^{-1} and 41.4 kJ mol^{-1} for Na^+ ion, and 5.2×10^{-11} m^2 s^{-1} and 36.8 kJ mol^{-1} for Cs^+ ion, which were close to those for water molecules in supercooled bulk water (1.6×10^{-10} m^2 s^{-1} and 44.4 kJ mol^{-1}, respectively [11]). These results suggest that not only HTO but also alkali cations may predominately diffuse through the capillary pore network which is partially plugged with the gel of hydrate.

Considering the remarkably larger sizes of hydrated cations (> 200 pm) compared to water molecules (O-H bond distance <100 pm), narrow regions may exist in which only HTO can access and diffuse but not Na^+ or Cs^+. If the case, the values of n are smaller for Na^+ and Cs^+ ions than for HTO, and the values of $F.F.$ are greater than for Na^+ and Cs^+ ions than for HTO. The discrepancies observed between the fitting curve and experimental data for Na^+ and Cs^+ ions may be caused by the use of the values of n and $F.F.$ obtained for HTO. A greater value of n will make the fitting curve steeper, and the effects of using the values of n and $F.F.$ obtained for HTO to model Na^+ and Cs^+ on the fitting can become at low w/c ratio where the n value is large even for HTO, leading to significant discrepancies observed at high temperature and high w/c ratio.

As conclusion, not only HTO but also alkali cations can be considered to diffuse mainly through capillary pores with a small volume of gel pores which is arranged in series in the direction of diffusion. However, a detailed evaluation of the diffusion behavior of cations in HCP, especially the degree of the contribution of gel pores, was impeded by the lack of parameters including activation energies of diffusion and diffusion coefficients of cations in supercooled bulk water (E_a^{R1}, D_v^{R1}). One way to estimate the values of D_v^{R1} and E_a^{R1} for cations may be molecular dynamics simulations. These values will enable further examination of the diffusion mechanisms of cations in HTO using the “serial model”.

Table 3-4 Apparent diffusion coefficients (D_a) and activation energies (E_a) for Na^+ and Cs^+ ions in HCP.

Tracer	w/c ratio	D_a [$\times 10^{-11}$ m^2 s^{-1}]				E_a
		293 K	303 K	313 K	323 K	[kJ mol^{-1}]
Na-22	0.36	0.50	0.66	1.1	2.1	34.1±2.8
		0.53	0.71	1.1	1.7	
	0.45	1.3	1.7	2.9	3.4	27.2±1.7
		1.2	1.7	2.7	3.3	
	0.60	3.4	4.4	5.6	5.9	14.8±1.3
		3.4	4.6	5.3	6.0	
Cs-137	0.36	0.57	1.3	1.5	2.1	31.3±4.0
		0.59	0.80	1.5	1.7	
	0.45	1.8	2.3	3.6	4.2	22.0±2.3
		1.8	2.3	3.7	3.6	
	0.60	4.6	5.7	7.5	10.0	18.7±1.7
		4.4	5.7	7.1	8.2	

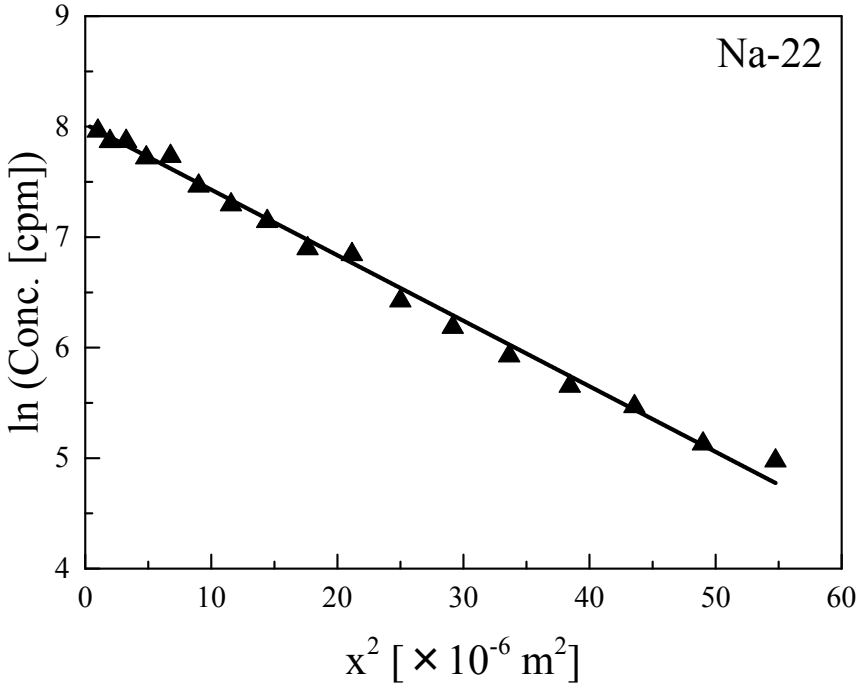

Figure 3-1 Concentration profile of diffusion for Na-22 (w/c ratio 0.45, at 303 K).

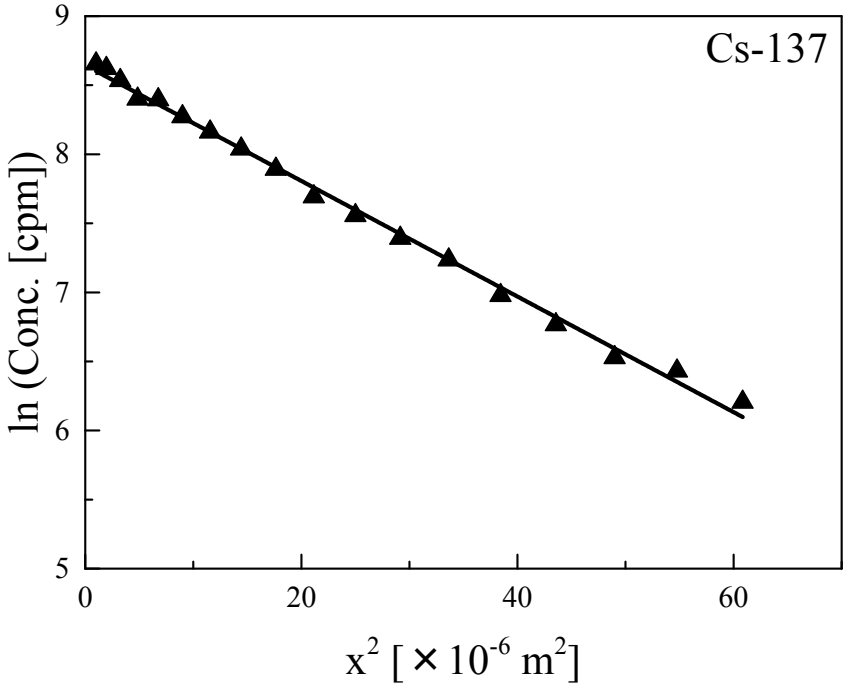

Figure 3-2 Concentration profile of diffusion for Cs-137 (w/c ratio 0.45, at 303 K).

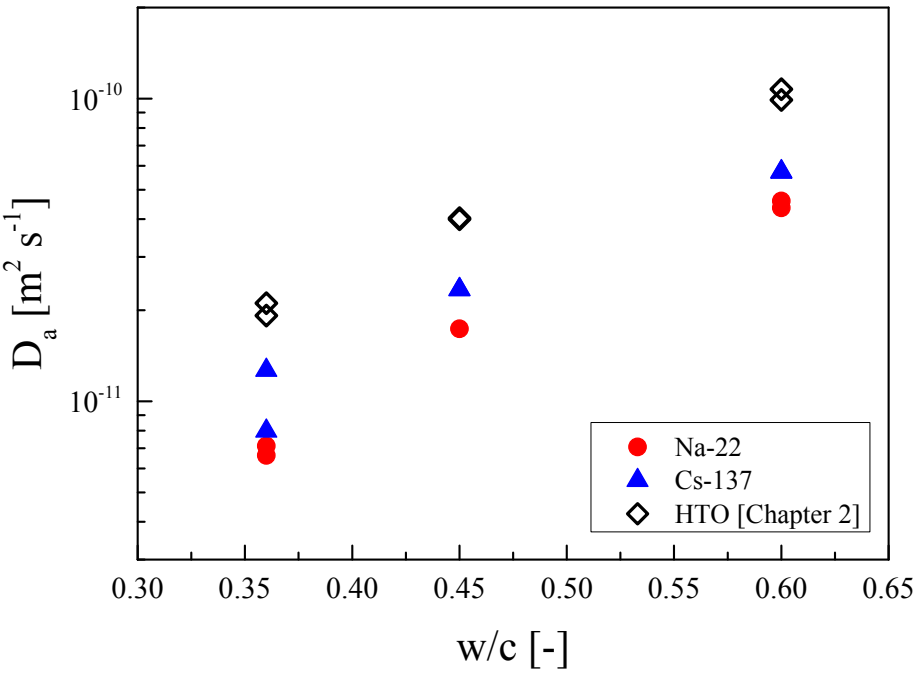

Figure 3-3 Dependence of the apparent diffusion coefficients for Na-22 and Cs-137 on w/c ratio.

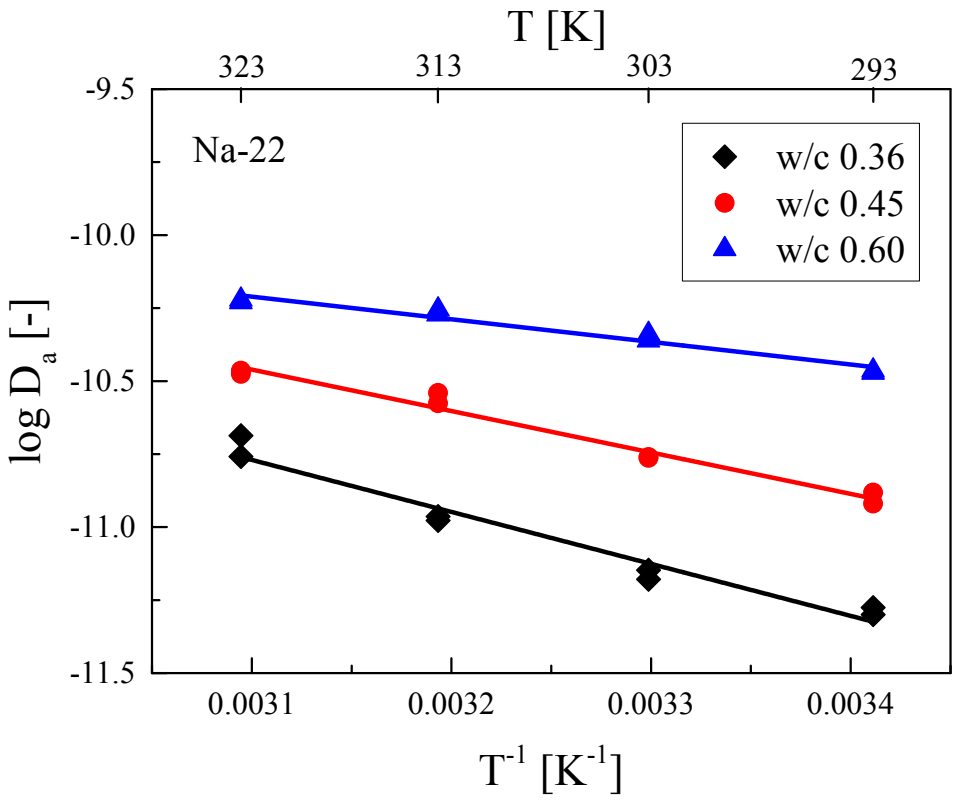

Figure 3-4 Dependence of the apparent diffusion coefficients of Na-22 on temperature.

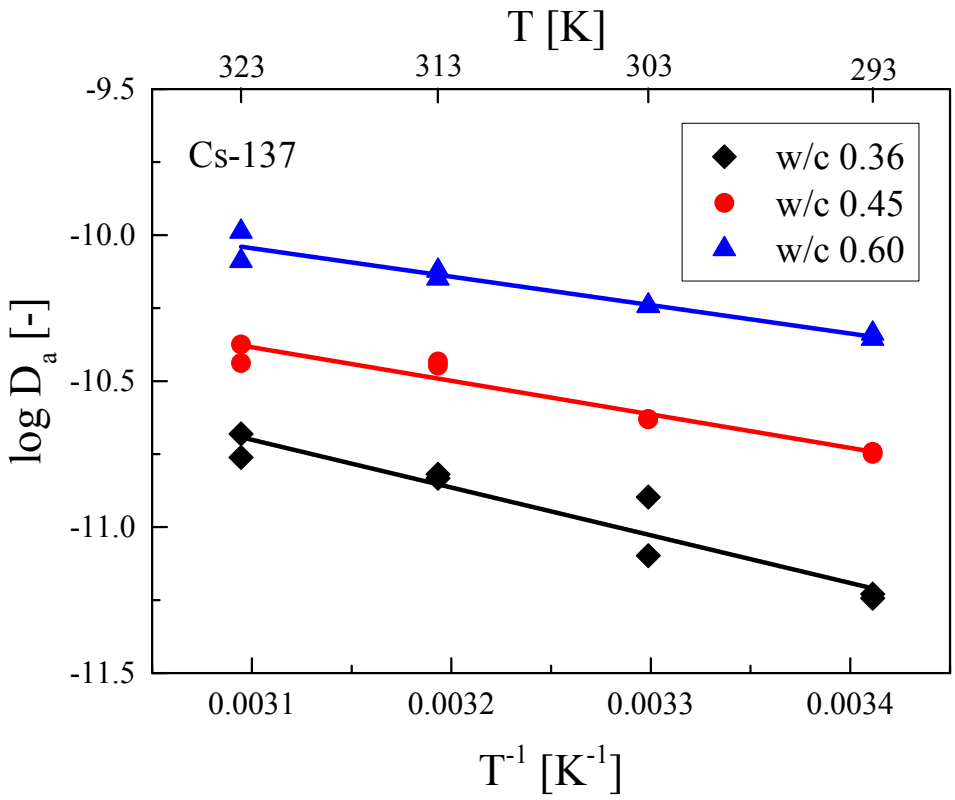

Figure 3-5 Dependence of the apparent diffusion coefficients of Cs-137 on temperature.

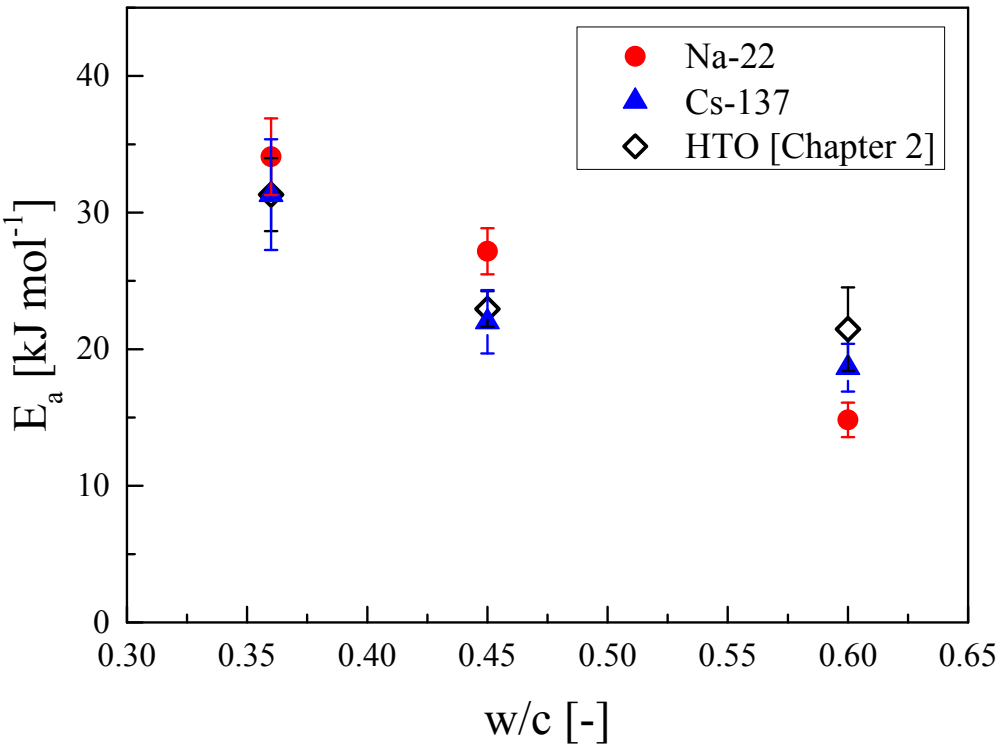

Figure 3-6 Dependence of the activation energies for Na^+ and Cs^+ diffusion on w/c ratio.

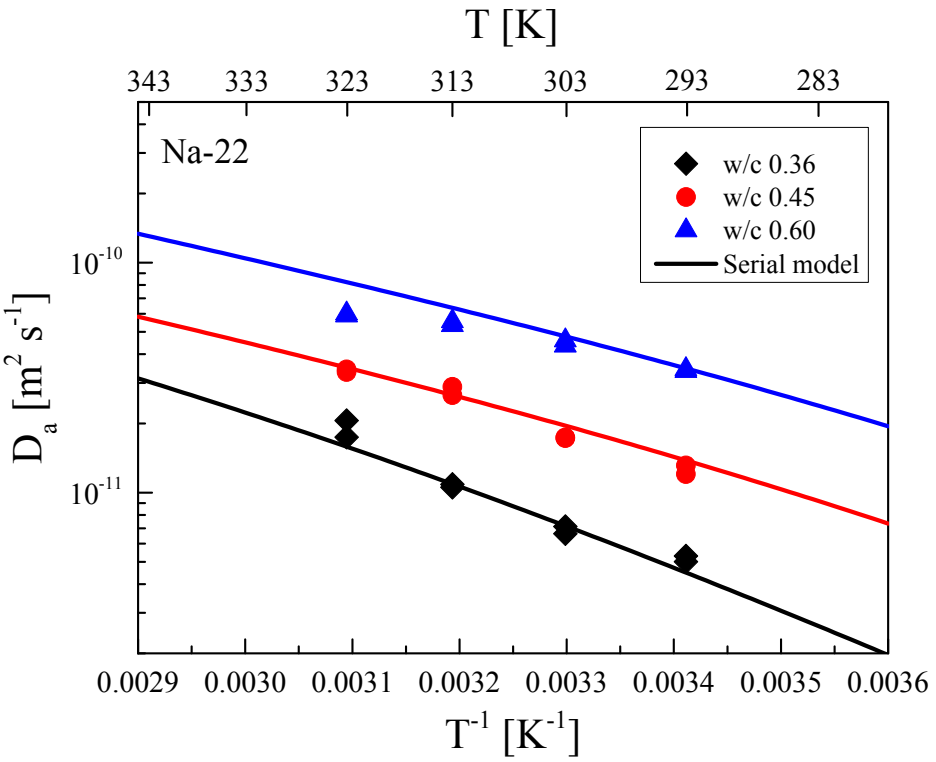

Figure 3-7 Fitting results for Na-22 by the serial model.

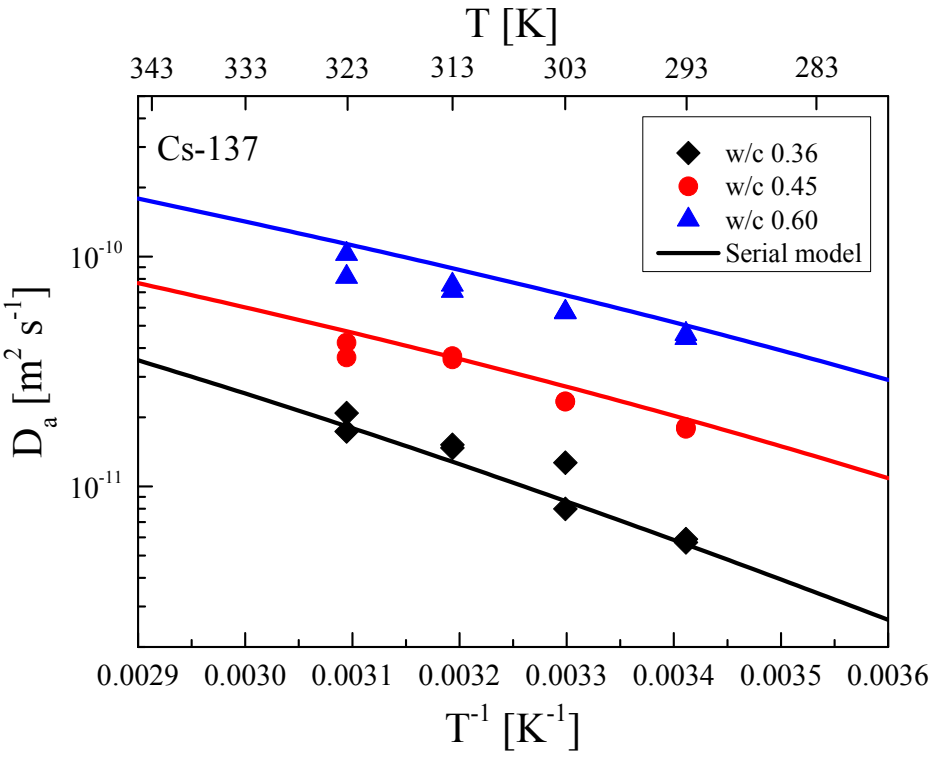

Figure 3-8 Fitting results for Cs-137 by the serial model.

3.4 Conclusions

In order to study the diffusion behavior of Na^+ and Cs^+ ions in HCP, the batch sorption experiment and the one-dimensional, non-steady diffusion experiment were conducted using Na-22 and Cs-137 as tracers. The batch sorption experiment revealed that neither Na^+ nor Cs^+ ions were sorbed on the HCP, and that no contribution of the sorption enthalpy on the activation energy for the diffusion of cations is expected. The apparent diffusion coefficients for Na^+ and Cs^+ ions obtained from the diffusion experiment increases with the increases in w/c ratio and temperature. The activation energies for the diffusion of Na^+ and Cs^+ ions, which were determined from the temperature dependence of the apparent diffusion coefficients at each w/c ratio, decreased from 34.1 kJ mol^{-1} to 14.8 kJ mol^{-1} for Na^+ ion and from 31.3 kJ mol^{-1} to 18.7 kJ mol^{-1} for Cs^+ ion when w/c ratio was increased from 0.36 to 0.60. These findings suggest that there are at least two diffusion processes for cations, similar to water, in HCP. The same diffusion model proposed for HTO, so-called “Serial model”, was examined by fitting with the experimental diffusion data of cations obtained in this study in order to clarify the diffusion mechanism. The fitting curve at each w/c ratio mostly reproduced the experimental data of the D_a for Na^+ and Cs^+ ions, suggesting that not only HTO but also alkali cations diffuse through mainly capillary pores with a small volume of gel pores which is arranged in series in the direction of diffusion. Because diffusion coefficients and activation energies of diffusion for Na^+ and Cs^+ ions in supercooled bulk water were not available, the n and $F.F.$ values obtained for HTO in Chapter 2 was used in Chapter 3. Further investigation into the diffusion coefficients and activation energies of cations in supercooled bulk water will enable the

more precise evaluation and interpretation of parameters n and $F.F.$ for Na^+ and Cs^+ ions in comparison to HTO, which may lead to a better understanding of the diffusion mechanisms of cations in the HCP.

References

[1] Japan Nuclear Cycle Development Institute and Federation of Electric Power Companies, JNC-TY1400 2005-001(1)/FEPC TRU-TR2-2005-03 in Japanese.

[2] Fujisaki K., Kubota S., Ueda H., Yamamoto T., Sugiyama D., Chida T., *Investigation of the methodology for selecting cementitious materials for the different components in the underground facility - Deriving component requirements and investigation of the weighting methodology*, Nuclear Waste Management Organization of Japan, NUMO-TR-13-07, 14-30 (2014).

[3] Page C. L., Short N. R., Tarras A. E., "Diffusion of Chloride Ions in Hardened Cement Pastes," *Cem. Concr. Res.*, **11**, 395-406 (1981).

[4] Goto S., Roy D. M., "Diffusion of ions through hardened cement pastes," *Cem. Concr. Res.*, **11**, 751-757 (1981).

[5] Ngala V. T., Page C. L., Parrott L. J., Yu S. W., "Diffusion in cementitious materials: II. Further investigation of chloride and oxygen diffusion in well-cured OPC and OPC/30% PFA pastes," *Cem. Concr. Res.*, **25**, 819-826 (1995).

[6] Hong S. –Y., Glasser F. P., "Alkali binding in cement pastes Part I. The C-S-H phase," *Cem. Concr. Res.*, **29**, 1893-1903 (1999).

[7] Faucon P., Charpentier T., Henocq P., Petit J. C., Virlet J., Adenot F., "Interaction of alkalis (Cs^+) with calcium silicates hydrates," *Mat. Res. Soc. Symp. Proc.*, **506**, 551-559 (1998).

[8] Wang J. H., Robinson C. V., Edelman I. S., "Self-diffusion and Structure of Liquid Water. III. Measurement of the Self-diffusion of Liquid Water with H^2, H^3 and O^{18} as Tracers," *J. Am. Chem. Soc.*, **75**, 466-470 (1953).

[9] Parsons R., *Handbook of Electrochemical Constants*, Butterworths Sci. Publ., London, p.79 (1959).

[10] Atkins P. W., *Physical Chemistry 6th ed.*, Oxford University Press, Oxford Melbourne Tokyo, p. 860 (1998).

[11] Price W. S., Hiroyuki I., Yoji A., "Self-Diffusion of Supercooled Water to 238 K Using PGSE NMR Diffusion Measurements," *J. Phys. Chem. A*, **103**, 448-450 (1999).

Chapter 4
Water-to-cement ratio dependence of diffusion behavior of Cl^- ion in hardened cement pastes

4.1 Introduction

Radioactive waste contains radionuclides with relatively long half-life which can dissolve as anionic species in groundwater. For the safety assessment of the radioactive waste disposal, migration behavior of such anionic species in the cement-based materials needs to be studied in detail as well as water and cations. However, the AFm (alumino-ferrite monosulfate hydrate) phase in the HCP are known to have ability to sorb anionic species on their surface by ion exchange with sulfate ion [1], which can lead to the formation of other phases such as Friedel's salt or Kuzel's salt [2-4]. Therefore, unlike HTO and cations, these chemical reactions should be considered when diffusion behavior of anion in the HCP is studied.

Chloride is a chemically stable monovalent anion, and its radioisotope, Cl-36, is a key radionuclide in the radioactive waste disposal since it can be generated in a nuclear reactor and has long half-life of 3.08×10^5 years. In addition, chloride is an important chemical species to affect the corrosion of an iron reinforcing bar in reinforced concrete. From these viewpoints, diffusion coefficients of chloride ions in cement-based materials have been experimentally determined [5-7], together with chemical and electrochemical characteristics of the cement hydrate surface so as to understand the diffusion behavior of chloride ions in the cement-based materials [2, 3, 8-10]. However, diffusion mechanism of chloride ions in the HCP is still being

discussed due to the complexities of chemical reactions and the microstructure of the potential diffusion pathways in HCP.

In this chapter, batch sorption experiments using Cl-36 as radiotracer were conducted under different temperature conditions similar to the cations in Chapter 3 so as to obtain information on the chemical reactions and sorption ability of the HCP with Cl^- ions. In addition, diffusion coefficients and the activation energies were determined from the diffusion experiments using Cl-36. Diffusion mechanism of Cl^- in the HCP, especially applicability of the "Serial model" to the Cl^- diffusion, was discussed based on the changes in the activation energy for the diffusion and the sorption enthalpy as a function of the w/c ratio.

4.2 Experimental methods

4.2.1 Preparation of HCP samples

The HCP samples were prepared and characterized by the same methods described in Section 2.2.1 and 2.2.2, respectively. The density (ρ) degree of hydration (α), total porosity (ε_{tot}), capillary porosity (ε_{cap}), and gel porosity (ε_{gel}) for HCP samples used in the sorption and diffusion experiments are shown in **Table 4-1**.

4.2.2 Batch sorption

The batch sorption experiment of Cl^- ion was performed by the same method described in Section 3.2.2. The initial Cl concentration in liquid phase was set to 10^{-2} mM by adding 20 μl of 5×10^{-3} M NaCl solution labeled with Cl-36. Radiotracer of Cl-36 (American Radiolabeled Chemicals Inc.) was obtained from Japan Radioisotope Association (JRIA). Sorption experiments were conducted at temperature from 293 to 323 K for a period of time ranging from 1 to 35 days. The radioactivity of Cl-36 in liquid phase was measured with a liquid scintillation counter (LSC-5100, Aloka, Ltd.).

4.2.3 Non-steady diffusion method

The apparent diffusion coefficients (D_a) of Cl^- ions in the HCP with different w/c ratios were determined by non-steady diffusion method with an instantaneous source (Cl-36), as described in Section 2.2.3. Tracer solution of 2×10^{-6} M NaCl labeled with Cl-36 was spiked on one side of the cylindrical shaped HCP sample. The amount of radiotracer spiked on the HCP was 450 Bq. After the diffusion from 4 to 48 days, the HCP samples were powdered with emery paper to obtain specimen from sections which

are 0.20-0.50 mm thick from the side of the HCP sample where the radiotracer was applied. The radiotracer of Cl-36 was then extracted by immersing the powdered HCP specimen into 0.5 M HNO_3 solution for more than 1 day. The radioactivity of Cl-36 extracted from the HNO_3 solution was determined with a liquid scintillation counter (LSC-5100, Aloka, Ltd.) after HNO_3 solution was neutralized with NaOH solution and mixed with a scintillator (InstaGel, Pakard, Ltd.). The radiotracer of Cl-36 used for the diffusion experiments was the same as the radiotracer used for the sorption experiments. The HCP samples were characterized before and after the diffusion experiments by the methods described the Section 2.2.2 so as to confirm the samples were not deteriorated during the diffusion.

Table 4-1 **Density (ρ), degree of hydration (α), total porosity (ε_{tot}), capillary porosity (ε_{cap}), and gel porosity (ε_{gel}) for HCP used in experiments.**

w/c ratio [-]	ρ [g cm^3]	α [-]	ε_{tot} [-]	ε_{cap} [-]	ε_{gel} [-]
0.36	1.83	0.713	0.287	0.152	0.136
0.45	1.63	0.772	0.341	0.223	0.117
0.60	1.41	0.829	0.414	0.328	0.086

4.3 Results and discussion

4.3.1 Sorption of Cl^- ion on HCP

In the batch sorption experiments, the radiotracer concentration of Cl-36 in liquid phase decreased for a period of time, until it reached constant after 21 days, suggesting chemical equilibrium state was attained by 21 days. The distribution coefficient, K_d, can be determined from the initial concentration (C_0) and the equilibrated concentration (C_{eq}) of the radiotracer in the liquid phase by the equation (3-1). It is noted that the K_d values obtained in this study may not represent only an equilibrium state of Cl^- sorption on the HCP, since chlorine can react with AFm phase to form other solid phase such as Friedel's salt and Kuzel's salt [2-4]. Therefore, hereafter, the apparent distribution coefficient, K_d^{app}, is used instead of the distribution coefficient, K_d, in this chapter.

The apparent distribution coefficients (K_d^{app}) for Cl^- ion obtained are listed in **Table 4-2**. The K_d^{app} value for the HCP sample ranged from 27.3 to 35.3 ml g^{-1} at w/c of 0.36, from 16.0 to 22.9 ml g^{-1} at w/c of 0.45, and from 11.6 to 22.3 ml g^{-1} at w/c of 0.60. The K_d^{app} values decreased with an increase in w/c ratio, and with decrease in sorption temperature. **Figure 4-1** shows the dependences of the K_d^{app} values on temperature at each w/c ratio, together with regression lines determined by the least-squares method. A good linearity was identified for the K_d^{app} values. Based on the temperature dependence of the K_d^{app} values, the apparent sorption enthalpy (ΔH^{app}) was determined using Van't Hoff equation (Equation (3-5)). The apparent sorption enthalpy (ΔH^{app}) obtained in this study are shown in **Table 4-2**. The ΔH^{app} values were positive ranging from 2.7 ± 1.4 to 11.3 ± 1.9 kJ mol^{-1} and increased with an

increase in w/c ratio, suggesting that the overall reaction is endothermic.

Chloride ion is known to sorb on C-S-H [3] and AFm phase in the HCP [2, 3]. In the case of sorption on the C-S-H phase, calcium ion bridges a silanol site of the C-S-H phase and a chloride ion as follows [8-10]:

$$\equiv \mathrm{SiOH} + \mathrm{Ca}^{2+} + \mathrm{Cl}^{-} \Leftrightarrow \equiv \mathrm{SiOCaCl} + \mathrm{H}^{+}, \qquad (4\text{-}1)$$

The equilibrium constant ($\log K$) of this reaction is −8.90 [8]. On the other hand, chloride ions and the AFm phase can react to form Kuzel's salt ($3\mathrm{CaO}\cdot(\mathrm{Al_2O_3/Fe_2O_3})\cdot 0.5\mathrm{CaCl_2}\cdot 0.5\mathrm{CaSO_4}\cdot 10\mathrm{H_2O}$) or Friedel's salt ($3\mathrm{CaO}\cdot(\mathrm{Al_2O_3/Fe_2O_3})\cdot\mathrm{CaCl_2}\cdot 10\mathrm{H_2O}$) under high Cl^- concentration [2, 3]. These formations of the salt can reduce the diffusion coefficient of Cl^- ion in the HCP if they occur even at low Cl^- concentration (10^{-5} M for sorption experiments, and 2×10^{-6} M for diffusion experiments in this study). Positive sorption enthalpy for Cl^- ion on the HCP is likely to be observed for the formation of Fe-Friedel's salt, of which the equilibrium constants and enthalpy are 12.91 and 174.8 kJ mol^{-1} [8].

4.3.2 Diffusion coefficients of Cl^- ion

A typical concentration profile of $^{36}Cl^-$ ion obtained in a diffusion experiment is shown in **Figure 4-2**. A good linearity was obtained in all cases when the logarithm of the tracer concentration was plotted as a function of x^2. The apparent diffusion coefficients (D_a) of Cl^- ion in the HCP were determined in the same way as described in section 2.3.2, and are listed in **Table 4-3**. The D_a values of Cl^- ion ranged from 5.0×10^{-14} m^2 s^{-1} to 3.2×10^{-12} m^2 s^{-1} at w/c ratio from 0.36 to 0.60 and at diffusion temperature from 293 to 323 K.

Figure 4-3 shows the D_a values of Cl^- ion at 303 K as a function of w/c ratio, together with those of HTO. It is noted that the D_a values of Cl^- ion is approximately two-order smaller than those of HTO, although Cl^- ion and HTO have almost the same diffusivity in bulk liquid water (2.03×10^{-9} m^2 s^{-1} for Cl^- [11] and 2.4×10^{-9} m^2 s^{-1} for HTO[12]). This finding suggests that Cl^- ions in HCP are significantly retarded in the HCP, probably due to high apparent distribution coefficient.

4.3.3 Activation energy for the diffusion of Cl^- ion

Figure 4-4 shows Arrhenius plots of the D_a values of Cl^- ion in the HCP at each w/c ratio, together with regression lines determined by the least-squares method. A good linearity was identified for the D_a values of Cl^- ion at each w/c ratio, suggesting the diffusion is dominated by a single process which can be described by the Arrhenius equation, i.e. Equation (2-10) in Chapter 2. The E_a values obtained for Cl^- ion are listed in **Table 4-3**. The E_a values for Cl^- ion increased with a decrease in w/c ratio as same as HTO in Chapter 2, Na^+ and Cs^+ ions in Chapter 3.

4.3.4 Diffusion mechanism of Cl^- ion in HCP

As discussed in the previous chapter, E_a value obtained from the temperature dependence of the D_a values may contain the contribution of the sorption enthalpy (ΔH). In case of Cl^- ion, this contribution cannot be ignored since the values of the sorption enthalpy obtained in the batch sorption experiments were positive. In this chapter, therefore, the net value of activation energy, E_a^{net}, for the Cl^- diffusion was calculated by subtracting the apparent sorption enthalpy from the activation energy

obtained in the diffusion experiments, according to the equation (3-4). The E_a^{net} values are listed in **Table 4-3**. The E_a^{net} values ranged between 50.9±4.2 (at w/c of 0.60) and 64.2±7.9 kJ mol^{-1} (at w/c of 0.36), and were significantly higher than the E_a value in bulk liquid water (17.4 kJ mol^{-1} [11]). This high activation energy indicates that unlike HTO and cations, capillary pores filled with water similar to bulk liquid water are not the predominant pathway for chloride diffusion in the HCP even at high w/c ratio.

According to the "Serial model" discussed in Chapters 2 and 3, the HCP sample has diffusion pathways of capillary pores and gel pores arranged in series in the direction of diffusion, and the dominant pathway for HTO and cations mostly consists of capillary pores. However, considering relatively high K_d^{app} value of Cl^- ion, only a small fraction of Cl^- ions, less than 3%, is present in the liquid phase; most of the Cl^- ion are on the solid phase either sorbed on HCP or formed other solid phase. When most of Cl^- ions are distributed in or on solid phase, bulk liquid water in capillary pores cannot work as dominant diffusion pathway; the net activation energy obtained for the Cl^- diffusion can be attributed to the movements of Cl^- ions on the surface of the solid phase which is covered by the supercooled liquid water. On the other hand, if high concentration of Cl^- ion is introduced to the HCP as tracer, it is likely that the diffusion coefficient of Cl^- ion increases and its activation energy decreases since the high concentration of the tracer can decrease the distribution coefficient, resulting in the increase in the contribution of the bulk liquid water to the Cl^- diffusion. When all the sorption/reaction sites are filled, Cl^- diffusion in capillary pores become dominant and the diffusion coefficient and the activation energy will approach the values in the bulk liquid water. Page et al. [5] conducted through-type diffusion experiments in which the

HCP sample was continuously contacted with a high concentration of Cl^- (1 M NaCl solution), and reported the activation energy for the effective diffusion of Cl^- ion which does not include the sorption enthalpy, i.e. corresponding to the net activation energy. The reported values of 41.8 ± 4.0 kJ mol^{-1} at w/c ratio of 0.40, 44.6 ± 4.3 kJ mol^{-1} at w/c ratio of 0.50, and 32.0 ± 2.4 kJ mol^{-1} at w/c ratio of 0.60 were slightly lower than the values obtained in this study (about 55 kJ mol^{-1}). This discrepancy is likely to be caused by the orders of magnitude difference in Cl^- concentration applied to the HCP.

In conclusion, the predominant diffusion pathway for Cl^- ion in the HCP is not bulk liquid water in capillary pores. The "Serial diffusion model" cannot be used to explain the diffusion coefficients of the Cl^- ion obtained under low tracer concentration condition, but the model may be applied for diffusion behavior of Cl^- ion under high tracer concentration condition.

Table 4-2 Apparent Distribution coefficient (K_d^{app}) and enthalpy (ΔH^{app}) for apparent sorption of Cl^- ion on HCP.

w/c ratio	K_d^{app} [ml g^{-1}]				ΔH^{app}
[-]	293	303	313	323	[kJ mol^{-1}]
0.36	27.3	34.1	31.6	32.1	2.7±1.4
	30.4	30.2	32.5	29.9	
	28.5	31.0	35.3	30.3	
0.45	16.9	17.5	21.7	21.6	8.0±1.7
	17.0	18.2	22.3	22.5	
	16.0	18.7	21.1	22.9	
0.60	11.6	14.5	18.2	22.3	11.3±1.9
	14.0	14.6	17.5	19.3	
	13.9	14.6	14.9	16.3	

Table 4-3 Apparent diffusion coefficients (D_a) and activation energy (E_a and E_a^{net}) for Cl^- ion in HCP.

w/c ratio	D_a [$\times 10^{-13}$ m^2 s^{-1}]				E_a	E_a^{net}
[-]	293 K	303 K	313 K	323 K	[kJ mol^{-1}]	[kJ mol^{-1}]
0.36	0.66	0.89	2.0	5.0	61.5±7.7	64.2±7.9
	0.50	0.81	1.9	5.2		
	—	—	3.9	—		
	—	—	3.9	—		
0.45	1.4	2.2	6.2	7.6	50.2±4.4	58.2±4.7
	1.3	2.0	5.3	9.0		
0.60	7.8	14.0	16.0	31.0	39.6±3.7	50.9±4.2
	5.6	12.0	20.0	32.0		

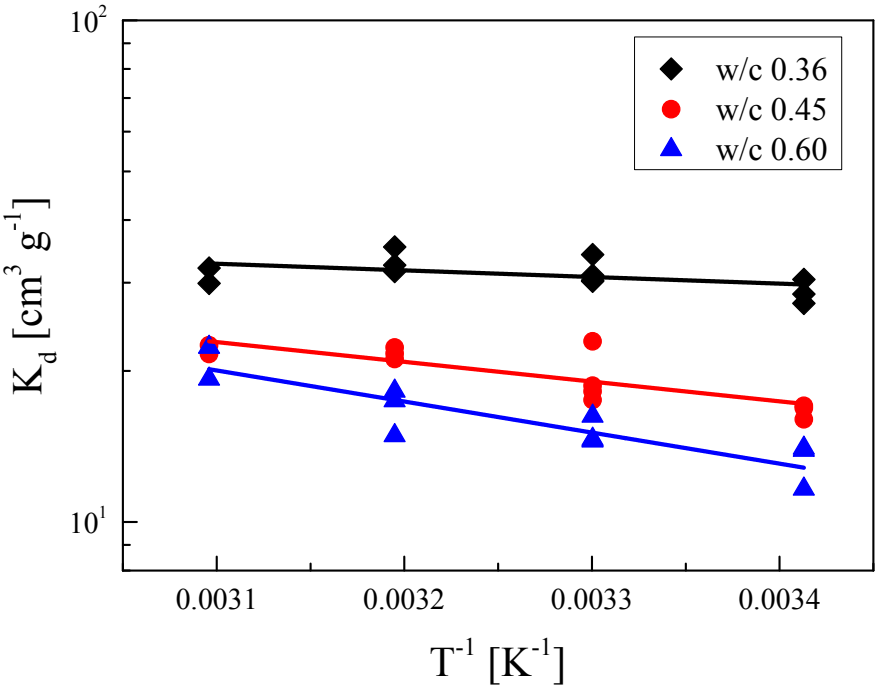

Figure 4-1 **Dependence of distribution coefficient for Cl^- ion on temperature at w/c ratio of 0.36, 0.45, and 0.60.**

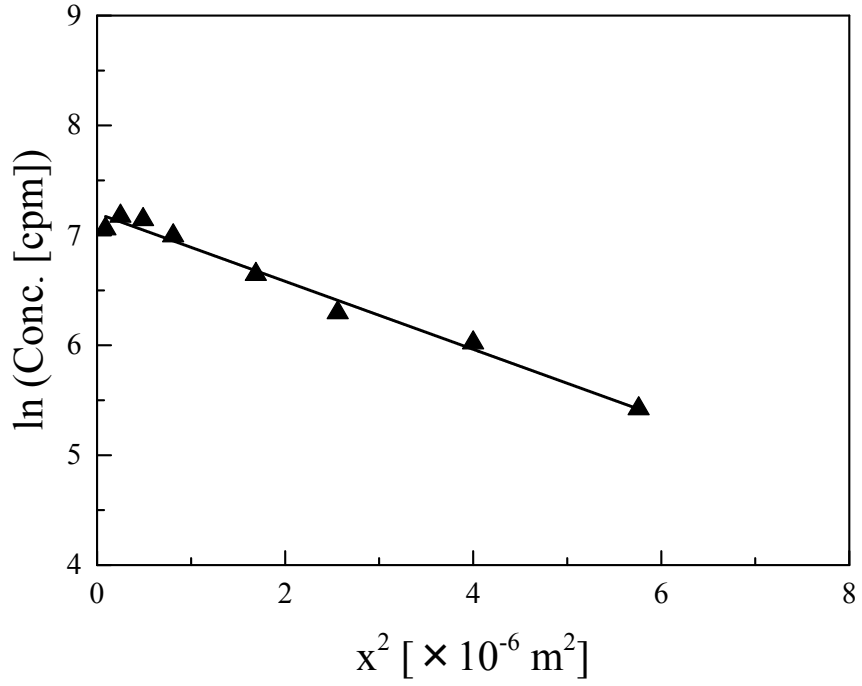

Figure 4-2 Concentration profile for Cl-36 for the instantaneous source (w/c ratio 0.45, at 303 K)

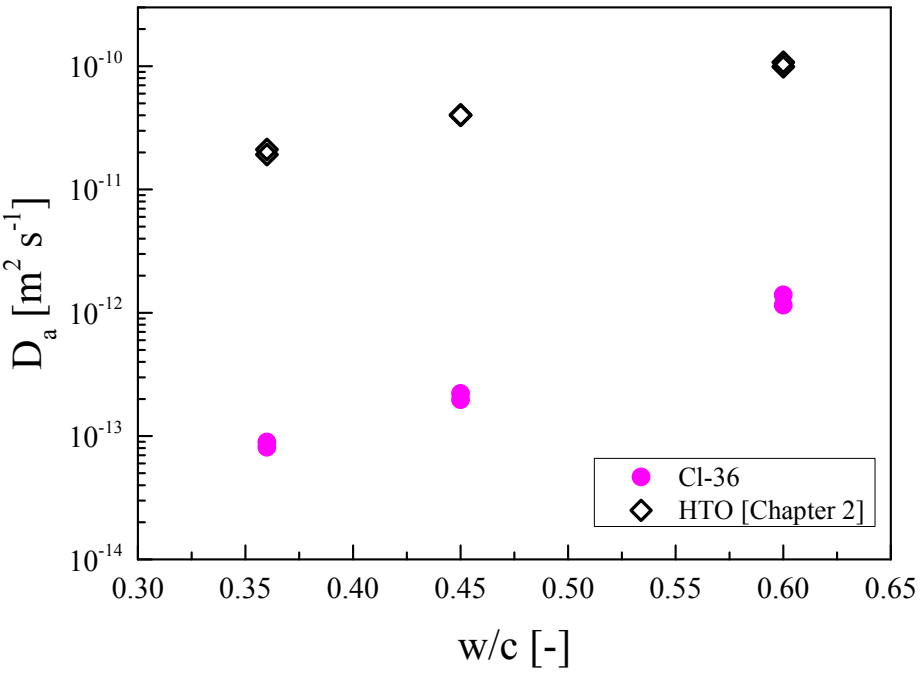

Figure 4-3 Dependence of the apparent diffusion coefficients for Cl^- ion on w/c ratio.

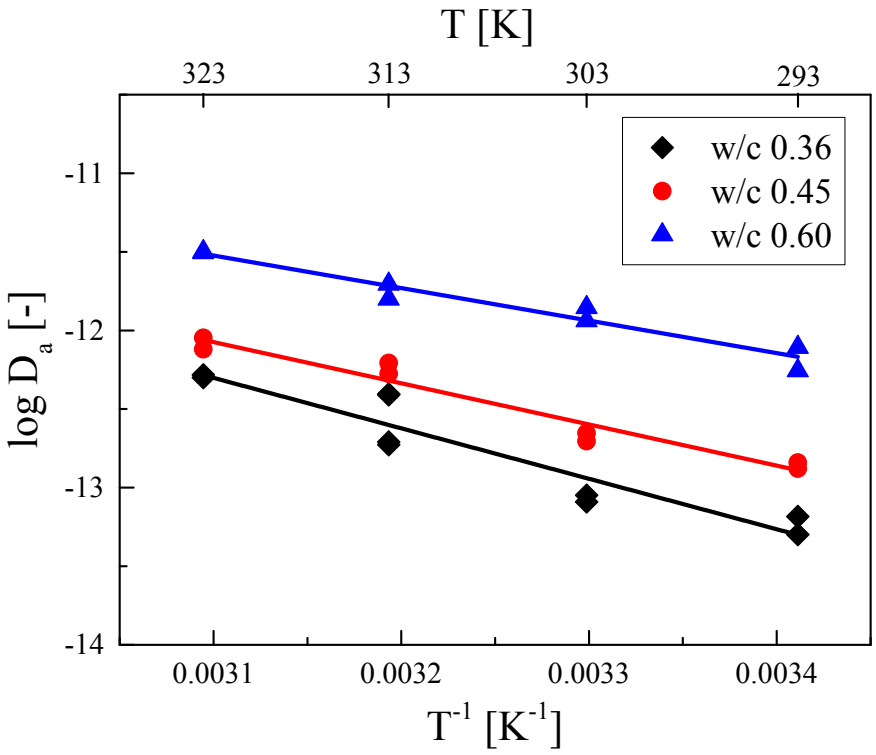

Figure 4-4 **Arrhenius plots of the apparent diffusion coefficients of Cl^- ion in HCP at w/c ratio of 0.36, 0.45, and 0.60.**

4.4 Conclusions

In order to study the diffusion of Cl^- ion in HCP, the batch sorption and non-steady diffusion experiments were conducted at different temperature from 293 to 323 K using Cl-36 as a tracer for the HCP samples prepared at w/c ratio from 0.36 to 0.60. The apparent distribution coefficient of Cl^- ion on the HCP ranged from 11.6 to 35.3 ml g^{-1} at w/c ratio of from 0.36 to 0.60, and it decreased with the increases in w/c ratio and temperature. The apparent sorption enthalpy determined from the temperature dependence of the distribution coefficients increased from 2.7 to 11.3 kJ mol^{-1} as the w/c ratio increased from 0.36 to 0.60. The apparent sorption of Cl^- ion on HCP was found to be an endothermic process.

The apparent diffusion coefficient obtained in this study ranged from 5.0×10^{-14} m^2 s^{-1} to 3.2×10^{-12} m^2 s^{-1} at w/c ratio from 0.36 to 0.60. It increased with the increases in the w/c ratio and the diffusion temperature. The activation energy for the diffusion of Cl^- ion in HCP decreased from 61.5 to 39.6 kJ mol^{-1} with an increase in the w/c ratio from 0.36 to 0.60. The net activation energy for diffusion is higher than the activation energy of diffusion in bulk liquid water, suggesting the bulk liquid water in the capillary pores is not the predominant diffusion pathway for Cl^- ion. The “serial model” cannot be applied to the Cl^- diffusion at least at low tracer concentration when most of Cl^- ions are on the solid phase, and do not exist in bulk liquid water.

References

[1] Mindess S., Young J. F., Darwin D., *Concrete 2nd ed.*, Prentice Hall, Pearson Education Inc., Upper Saddle River, New Jersey, 57-91 (2003).

[2] Zibara H., "Binding of external chlorides by cement pastes," *Thesis (PhD)*, University of Toronto.

[3] Hirao H., Yamada K., Takahashi H., Zibara H., "Chloride binding od cement estimated by binding isotherms of hydrates," *J. Adv. Concr. Technol.*, **3**, 77-84 (2005).

[4] Glasser F. P., Kindness A., Stronach S. A., "Stability and solubility relationships in AFm phases Part I. Shrolide, sulfate and hydroxide," *Cem. Concr. Res.*, **29**, 861-866 (1999).

[5] Page C. L., Short N. R., Tarras A. E., "Diffusion of Chloride Ions in Hardened Cement Pastes," *Cem. Concr. Res.*, **11**, 395-406 (1981).

[6] Goto S., Roy D. M., "Diffusion of ions through hardened cement pastes," *Cem. Concr. Res.*, **11**, 751-757 (1981).

[7] Ngala V. T., Page C. L., Parrott L. J., Yu S. W., "Diffusion in cementitious materials: II. Further investigation of chloride and oxygen diffusion in well-cured OPC and OPC/30% PFA pastes," *Cem. Concr. Res.*, **25**, 819-826 (1995).

[8] Kari O. P., Elakneswaran Y., Nawa T., Puttonen J., "A model for a long-term diffusion of multispecies in concrete based on ion-cement-hydrate interaction," *J. Mater. Sci.*, **48**, 4243-4259 (2013).

[9] Elakneswaran Y., Nawa T., Kurumisawa K., "Electrokinetic potential of hydrated cement in relation to adsorption of chlorides," *Cem. Concr. Res.*, **39**, 340-344 (2009).

[10] Elakneswaran Y., Iwasa A., Nawa T., Sato T., Kurumisawa K., "Ion-cement hydrate interactions govern multi-ionic transport model for cementitious materials," *Cem. Concr. Res.*, **40**, 1756-1765 (2010).

[11] Parsons R., *Handbook of Electrochemical Constants*, Butterworths Sci. Publ., London, p.79 (1959).

[12] Wang J. H., Robinson C. V., Edelman I. S., "Self-diffusion and Structure of Liquid Water. III. Measurement of the Self-diffusion of Liquid Water with H^2, H^3 and O^{18} as Tracers," *J. Am. Chem. Soc.*, **75**, 466-470 (1953).

Chapter 5
Conclusions

Cement-based materials will be used as barrier materials such as solidifications, fillers, and low diffusion layers for low-level radioactive waste disposal. On the other hand, alkaline components leached from cement-based materials, which is also used in large quantities as structural materials and grout for low-level and high-level radioactive waste disposal, are possible to deteriorate the performance of the other barrier materials (bentonite and geological features). Therefore, it is very important to elucidate the diffusion mechanisms of chemical species in cement-based materials in order to assess the barrier performance of cement-based materials and the influence of cement alkaline components on the other barrier materials (bentonite and geological features). This study is intended to give new insight into the diffusion mechanisms in hardened cement paste (HCP), as a basic study for the safety assessment of the disposal of both low-level and high-level radioactive waste.

In **Chapter 2**, the diffusion behavior of water was examined based on the dependence of apparent diffusion coefficients and activation energies on w/c ratio. The apparent diffusion coefficients of water were obtained as functions of w/c ratio and temperature using HTO as a tracer by a non-steady diffusion experiment. In addition, non-steady diffusion experiments using $H_2{}^{18}O$ as another tracer were also conducted in order to check the influence of dissociation products of HTO on diffusion. The apparent diffusion coefficients of HTO were in agreement with those of $H_2{}^{18}O$, suggesting that both HTO and $H_2{}^{18}O$ predominantly diffuse as H_2O molecule: the dissociation of water

molecule is not significant for HTO diffusion even in alkaline porewater in HCP. The apparent diffusion coefficients of HTO positively correlated with w/c ratio and temperature. The activation energy for diffusion was determined from the temperature dependence of apparent diffusion coefficients using Arrhenius equation. The activation energy at lower w/c ratio of 0.36 was higher than in bulk liquid water, while the activation energy at higher w/c ratio of 0.60 was close to that in bulk liquid water. The finding suggested that gel pores, which are filled with water similar to supercooled bulk water, contribute to HTO diffusion in HCP in addition to capillary pores filled with bulk liquid water. Two diffusion models consisting of capillary and gel pores were proposed based on the microstructure of HCP and the nature of water in pores. By optimizing the model to the experimental data, a degree of the contribution of gel pores to diffusion and the pore geometry were examined. The result showed that dominant diffusion pathway of water in HCP is a pore network mostly consisting of capillary pores plugged with a very small part of gel pores.

In **Chapter 3**, the diffusion behaviors of cations were examined using Na-22 and Cs-137 as tracers by batch sorption and non-steady diffusion experiments. The batch sorption experiment revealed no sorption of Na^+ and Cs^+ ions on HCP and no contribution of sorption enthalpy on the activation energy for the diffusion. The apparent diffusion coefficients of Na^+ and Cs^+ ions increased with increases in w/c ratio and temperature. The activation energies for Na^+ and Cs^+ diffusion in HCP at higher w/c ratio were close to those in bulk liquid water, and increased with a decrease in w/c ratio, similar to the results of HTO. This finding suggested that gel pores contribute to Na^+ and Cs^+ diffusion in HCP, similar to HTO. The experimental data of Na^+ and Cs^+

diffusion can be mostly reproduced by applying the same diffusion model (i.e. serial model) developed in Chapter 2, suggesting that Na^+ and Cs^+ ions also diffuses mainly through the capillary pore network plugged by a very small part of gel pores.

In **Chapter 4**, the diffusion behavior of anions was examined using Cl-36 as a tracer by batch sorption and non-steady diffusion experiments. The apparent distribution coefficients increased with a decrease in w/c ratio and an increase in temperature. The apparent sorption enthalpies, which were determined from the temperature dependence of the apparent distribution coefficients, were positive in all cases of w/c ratio, indicating that the sorption of Cl^- ion on HCP was an endothermic process. The apparent diffusion coefficients increased with increases in w/c ratio and temperature. The apparent activation energy for Cl^- diffusion increased with a decrease in w/c ratio similar to the results of HTO, Na^+, and Cs^+ ions. However, the net activation energies for Cl^- diffusion, which were determined by subtracting sorption enthalpies from apparent activation energies, were significantly higher than in bulk liquid water even at higher w/c ratio. This finding suggests that capillary pores filled with bulk liquid water were not the predominant diffusion pathway, and the "serial model" developed in Chapter 2 for HTO cannot be applied to the diffusion of chemical species that are mostly sorbed to cement hydrates and do not exist in the liquid phase.

This thesis provided new findings on the relationship of diffusion of neutral species (HTO) and ionic species to microstructure of HCP filled with water of different nature from the viewpoint of the activation energy for diffusion. Assuming capillary pores are filled with free water while gel pores are filled with water similar to supercooled bulk water, the higher activation energy of diffusion suggests a contribution

of gel pores and the degree of contribution of gel pores was evaluated using a model. This analysis revealed that dominant diffusion pathway for neutral species and cations are mostly capillary pores with a very small contribution of gel pores. The volume of gel pore that participates in diffusion is much smaller than the actual volume of gel pores in HCP determined experimentally, suggesting that only the gel pores that plug capillary pores contribute to diffusion. Analysis of sorption, diffusion, and activation energy results of anions showed that capillary pores filled with bulk liquid water were not the predominant diffusion pathway for anions. This approach of examining the activation energy of diffusion developed in this thesis will also enable us to elucidate the diffusion behavior of chemical species in other types of cementitious materials. The findings in this thesis on the diffusion in cementitious materials may be able to contribute not only to a reliable performance assessment of the radioactive waste disposal but also to studies of the physical and chemical properties of cement-based materials used in other fields.

Acknowledgements

The thesis is a summary of the results in my researches for a doctoral course at Laboratory of Nuclear and Environmental Materials, Division of Energy and Environmental Systems, Graduate School of Engineering, Hokkaido University.

My deepest appreciation first goes to supervisor Professor Tamotsu Kozaki, who provided me the best environment for the researches and constructive advices for the achievement of the present thesis. What I have learned from him is certainly essential for me to be a good researcher.

I would like to express my sincere gratitude to Professors Hideyuki Ogawa and Takafumi Sugiyama for their reviewing this thesis and giving useful directions. I would like to express my profound gratitude to Associate Professor Naoko Watanabe from the laboratory for not only reviewing this thesis but also many constructive comments and warm encouragement. I am deeply grateful to Assistant Professor Shingo Tanaka from the laboratory, for many advices and words of encouragement. I also thank my former supervisor, Professor Seichi Sato for giving me various advices for my research and providing me an opportunity to study not only on radioactive waste disposal but also on nuclear fuel cycle while I was in undergraduate and master's courses.

All the radioisotopes experiments were carried out at Central Institute of Isotope Science, Hokkaido University. I would like to thank Professor Shigetsugu Hatakeyama and the staffs of the Institute for their help.

I wish to express my cordial gratitude to the secretaries in the lab, Mses. Takako Okuyama, Yuka Iwataki, and Aki Chiba (Inugai), who have provided a clerical

support. I sincerely would like to acknowledge all of my colleagues in the Laboratory of Nuclear and Environmental Materials, Ms. Haruna Kobayashi, and Messrs. Takanori Chiba, Akihiro Matsuki, Yusuke Iwano, Yasuhiro Ikuta, Kota Tsugawa, Daisaku Shitara, Jaka Rachmadetin, Ryoichi Hojo, Kai Hashibe, Hiroi Yamazaki, Ryohei Miyoshi, and Yuli Purwanto, for their selfless cooperation, numerous experimental supports and suggestive discussions. They made my life as a graduate student enjoyable with fun and relaxing conversations and comfortable and warm atmosphere in the lab.

Finally, my hearty appreciation goes to my dear father, mother and sister who have selflessly and continuously provided emotional and financial supports.